University of Szeged
Faculty of Pharmacy
Institute of Pharmaceutical Technology and Regulatory Affairs
Head: Dr. habil. Ildikó Csóka Ph.D.

Ph.D. Thesis

IMPROVED SKIN PENETRATION USING ACTIVE AND PASSIVE ENHANCEMENT METHODS

by

Mónika Bakonyi
pharmacist

Supervisors:

Dr. habil. Erzsébet Csányi Ph.D.
Dr. Szilvia Berkó Ph.D.

Szeged
2018

PUBLICATIONS RELATED TO THE SUBJECT OF THE THESIS

I. **Bakonyi Mónika**, Berkó Szilvia, Budai-Szűcs Mária, Kovács Anita, Spaits Tamás, Samu Gyöngyi, Csányi Erzsébet: *In vitro* bőrmodellek, mint a hatékony gyógyszerformulálás eszközei.
Acta Pharmaceutica Hungarica 87 3-12 (2017)

IF:-

II. **Mónika Bakonyi**, Szilvia Berkó, Mária Budai-Szűcs, Anita Kovács, Erzsébet Csányi: DSC for evaluating the encapsulation efficiency of lidocaine-loaded liposomes compared to the ultracentrifugation method.
Journal of Thermal Analysis and Calorimetry 130 (3) *1619-1625 (2017)*

IF:1.953 (2016)
Citations: 1

III. **Mónika Bakonyi**, Szilvia Berkó, Anita Kovács, Mária Budai-Szűcs, Nikolett Kis, Gábor Erős, Ildikó Csóka, Erzsébet Csányi: Application of Quality by Design principles in the development and evaluation of semisolid drug carrier systems for the transdermal delivery of lidocaine.
Journal of Drug Delivery Science and Technology 44 136-145 (2018)

IF: 1.194 (2016)

IV. **Mónika Bakonyi**, Attila Gácsi, Anita Kovács, Mária Budai-Szűcs, Szilvia Berkó, Erzsébet Csányi: Following-up skin penetration of lidocaine from different vehicles by Raman spectroscopic mapping.
Journal of Pharmaceutical and Biomedical Analysis 154 1-6 (2018)

IF: 3.255 (2016)

V. **Mónika Bako**nyi, Szilvia Berkó, Gábor Erős, Gábor Varjú, Christina Dehelean, Mária Budai-Szűcs, Erzsébet Csányi: A review of electroporation-based antitumor skin therapies and investigation of betulinic acid-loaded ointment.
Anti-cancer Agents in Medicinal Chemistry (accepted for publication) doi:10.2174/1871520617666171113120255

IF: 2.598 (2016)

VI. Petra Hartmann, Edina Butt, Ágnes Fehér, Ágnes Lilla Szilágyi, Kurszán Dávid Jász, Boglárka Balázs, **Mónika Bakonyi**, Szilvia Berkó, Gábor Erős, Mihály Boros, Gyöngyi Horváth, Endre Varga, Erzsébet Csányi: Electroporation-enhanced transdermal diclofenac sodium delivery into the knee joint in a rat model of acute arthritis. *Drug Design, Development and Therapy* (*accepted for publication*)

IF: 2.822 (2016)

PRESENTATIONS RELATED TO THE SUBJECT OF THESIS

I. Boglárka Balázs, **Mónika Bakonyi**, Szilvia Berkó, Mária Budai-Szűcs, Erzsébet Csányi: Non-invasive *in vivo* comparison of penetration enhancers containing hydrogel formulations. *1st European Conference on Pharmaceutics: Drug delivery.* Reims, France, 13-14. 04. 2015 (poster*)*

II. Berkó Szilvia, **Bakonyi Mónika**, Csányi Erzsébet: Bőrön keresztüli hatóanyagbevitel elektroporáció segítségével. *Gyógyszerkémiai és Gyógyszertechnológiai Szimpózium,* Herceghalom, Hungary, 15-16. 09. 2016 (verbal presentation)

III. Kovács Anita, Berkó Szilvia, **Bakonyi Mónika,** Kőrösi Zita, Csányi Erzsébet: Dermálisan alkalmazott kozmetikai készítmények fejlesztése és vizsgálata. *Kozmetikai Szimpózium,* Budapest, Hungary, 17. 11. 2016 (verbal presentation)

IV. **Mónika Bakonyi**, Szilvia Berkó, Erzsébet Csányi: Investigation of lidocaine base liposomes for transdermal delivery. *7th BBBB International Conference on Pharmaceutical Sciences*. Balatonfüred, Hungary, 5-7. 10. 2017, *Acta Pharmaceutica Hungarica 87 (043) (2017) (*poster)

V. **Mónika Bakonyi**, Szilvia Berkó, Erzsébet Csányi: Investigation of lidocaine-containing NLC systems for dermal application. *15th Annual European Pharma Congress*. Frankfurt, Germany, 7-9.05.2018, *Pharmaceutical Regulatory Affairs: Open Access 7 (2018) (*poster)

TABLE OF CONTENTS

ABBREVIATIONS

API	active pharmaceutical ingredient
BA	betulinic acid
CMA	critical material attribute
CPE	chemical penetration enhancer
CPP	critical process parameter
CQA	critical quality attribute
DSC	differential scanning calorimetry
ECT	electrochemotherapy
EE%	encapsulation efficiency
EP	electroporation
FT-IR	Fourier transform infrared spectroscopy
HEPES	4-(2-hydroxyethyl)-1-piperazineethanesulfonic acid
HPLC	high-performance liquid chromatography
HSE	heat separated epidermis
LID	lidocaine
LLC	lyotropic liquid crystal
NLC	nanostructured lipid carrier
PAMPA	parallel artificial membrane permeability assay
PBS	phosphate buffered saline
PVPA	phospholipid vesicle-based permeation assay
QbD	Quality by Design
QTPP	quality target product profile
RA	risk assessment
SC	stratum corneum
SCLL	stratum corneum lipid liposome
TEWL	transepidermal water loss

1. INTRODUCTION

The dermal delivery of active agents is an attractive alternative to conventional administration routes, especially when the pathological conditions intended to be treated are located in the skin. This administration route offers lower dosage and lower systematic toxicity with effective local concentration, in addition, it is a non-invasive and patient-friendly method [1]. Furthermore, topically applied drugs avoid hepatic first pass metabolism and the degradation in the gastrointestinal system if they are absorbed [2,3].

One of the most compelling medical challenges of this century is the treatment of cancer. Skin cancer has shown increasing incidence over the past decades for various reasons in connection with the increased ultraviolet radiation exposure, environmental and genetic factors [4]. Skin cancer at early stages is localized within the upper layers of skin, thus the dermal application of anticancer agents in the localized region is advantageous for the effective treatment of the tumor, such as for postoperative treatments.

Effective topical local anesthesia is also a challenge nowadays because most of the marketed topical formulations have moderate skin penetration properties, a rapid but short effect. Thus the development of local topical anesthetics with a prolonged release at the site of action is also desperately desired [5]. Both of the above-mentioned therapeutic goals require the penetration of the drugs into the dermal layers of the skin.

However, because of the barrier function of the outermost layer of the skin, the stratum corneum, only small and lipophilic molecules are able to penetrate through the skin by passive diffusion [6,7]. Numerous technologies have been developed to enhance the penetration of molecules through this barrier based on various strategies: increasing skin permeability, providing a driving force acting on the drug, or the combination of these methods. They can be categorized as passive and active approaches [8].

The selection of an adequate drug carrier system with proper material attributes and/or the application of active and passive penetration enhancement methods are/is fundamental to reaching the aim of application. With a rationalized, scientific and risk-based initial theoretical development before the technical development, parameters that most strongly influence the final formulation can be discovered and monitored. With the consideration of the Quality by Design approach related to the development of new pharmaceutical formulations, a cost-saving process ensuring a high-quality product taking into account patient expectations, industrial and regulatory aspects can be achieved.

2. LITERATURE BACKGROUND

2.1. The barrier function of the skin

The skin is composed of several well-defined layers. From the outside to the inside, the three main layers are the epidermis, the dermis and the subcutaneous tissues.

The barrier function of the skin is mostly provided by the outermost layer of the epidermis, the stratum corneum (SC). It is about 10–20 μm thick and acts as a barrier to exogenous substances as well as to water release from the deeper layers into the atmosphere, known as transepidermal water loss (TEWL) [9]. This function is due to the brick-mortar structure, where corneocytes are embedded in an intracellular lipid matrix organized as lamellar lipid layers [10]. Corneocytes are flat dead cells filled with keratin filaments and they are produced in the deepest layer of the epidermis, the stratum basale. Corneocytes migrate through the epidermis and undergo a number of changes in both structure and composition, and during this differentiation they synthesize and express numerous different structural proteins and lipids. The lipid matrix is predominantly composed of ceramides, cholesterol and free fatty acids, but small amounts of cholesterol sulfate and cholesterol esters are also present [11,12]. These lipids form a highly ordered gel phase membrane domain, which is the least permeable liquid crystalline counterpart of all [12].

2.2. Therapeutic aims of dermal drug delivery: anticancer and local anesthetic treatment

The dermal drug delivery of active agents is the most feasible when the target of therapy is located in the skin. In my Ph.D. work, we aimed at two therapeutic indications, which are receiving more and more attention nowadays: topical therapy of melanoma and local anesthesia.

2.2.1. Melanoma

Skin cancer is the most common type of cancer affecting Caucasian populations, and among various types, melanoma is the most aggressive form that can metastasize, and it has a much higher mortality rate than nonmelanoma skin cancers [13]. In the early stages, skin cancers develop in the outer layers of the skin. If not treated, they may grow deeper into the skin with the development of metastases. Anticancer drugs which are administered orally or by intravenous route are associated with serious side effects. Topical dosage forms deliver most of the drug locally with fewer side effects compared with other routes of administration, thus the dermal administration of chemotherapeutic drugs could offer a solution to the above-mentioned limitations [14]. This localized delivery also limits the exposure of healthy internal tissues to cytotoxic anticancer agents, and thus improves the quality of life of patients [15].

Furthermore, it has other benefits in the treatment of cancer, such as increased patient compliance, reduced surgical costs and lack of undesirable scars. Topical treatment is considered when the tumors are present in the upper layers of the skin and also for palliative treatment [14]. The development of anticancer formulations should be based on three keystones: the drug, the delivery system, and the type of cancer to be treated, to balance many different variables and maximize efficacy (Figure 1).

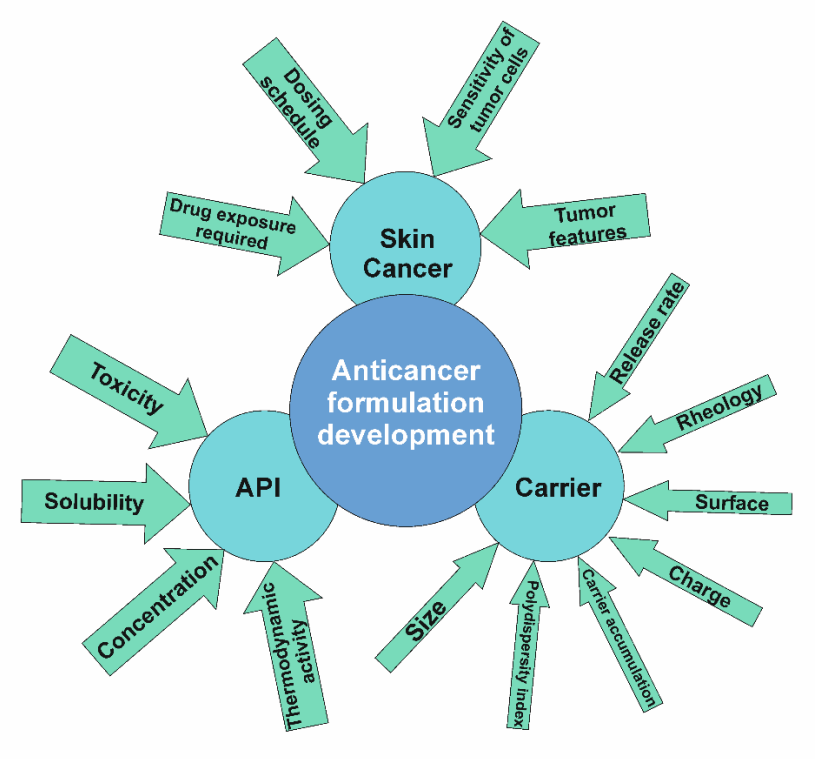

Fig. 1. Keystones in anticancer formulation development.

2.2.2. Local anesthesia

The application of local anesthetics, usually administered by subcutaneous injection, is common in the course of diagnostic, therapeutic, and cosmetic dermatology procedures. The effective dermal delivery of local anesthetics could offer a solution to many adverse effects caused by needle insertion, such as pain, local reactions or toxicity, and additionally, it avoids the disruption of anatomical landmarks. Therefore, innovative dermal formulations of local anesthetics are needed to overcome the barrier function of the skin and provide sufficient and prolonged local anesthesia.

Lidocaine (LID) is a local anesthetic agent used in pharmacological pain control and management. The site of action for LID is the dermis, which contains the free nerve endings responsible for pain sensation [16,17]. However, the topical application of this drug is not as effective as administration by subcutaneous injection because its penetration into the dermal layers is limited owing to the barrier function of the SC. Most of the marketed topical

formulations have moderate skin penetration properties, a rapid but short effect, thus the development of local topical anesthetics with a release in a prolonged fashion at the site of action is desperately desired [5]. Using a vehicle which maximizes drug delivery into the dermis seems to be a good strategy for optimizing the percutaneous permeation of topically applied drugs. So there is an urgent need for further research in this field, for the development of new systems that allow better penetration and prolonged anesthesia [18,19].

2.3. Trans/intradermal drug delivery strategies

The penetration and effectiveness of topically applied drugs are limited because of the barrier function of the skin's outermost layer, the SC. Several methods are used to increase penetration and reach sufficient concentration levels at the site of action: passive methods, such as the use of chemical penetration enhancers (CPEs), or the application of nanoparticle delivery systems and/or active methods.

2.3.1. Passive methods

2.3.1.1. Chemical penetration enhancers

To overcome the barrier function of the SC, CPEs are conventional and effective approaches as they reduce skin barrier resistance and thus promote the penetration of drugs [20,21].

The mechanism of action of CPEs is thought to be achieved by disrupting the packing of skin lipids and altering the barrier of the SC, by changing the partitioning behavior of the drug at the SC-viable epidermis interface or by affecting the thermodynamic activity of the drug [22,23].

In my Ph.D. work, two chemical penetration enhancers were investigated: Transcutol and Kolliphor RH40.

Transcutol, a monoethyl ether of diethylene glycol, is classified into the group of alcohols and glycols, which are reported to interact with the aqueous domain of the lipid bilayers, which increase the solubility of drugs in the skin [24]. Harrison et al. reported that the penetration enhancement property of Transcutol is the result of changes in solubility rather than diffusion in the membrane [25]. Another study stated that the enhancing ability of Transcutol is attributed to its ability to pass through the skin and get incorporated into the multiple lipid bilayers, thereby swelling the intercellular lipids [26]. These results suggest that further studies are required to elucidate its exact interaction with skin components.

Kolliphor RH40 (Polyoxyl 40 Hydrogenated Castor Oil) is a non-ionic surfactant reported to shift the drug distribution to the SC, but the exact mechanism has not been described yet [26,27]. Generally, non-ionic surfactants have low toxicity, however, they also have a minor

enhancement effect compared to ionic types, which could be explained by the low degree of the SC structure disordering effect [28].

2.3.1.2. Carrier systems

The effectiveness and acceptability of dermal formulations are directly related to the properties of the carrier used. The optimal vehicle can enhance penetration of the active agents, therefore promote the desired outcome.

Nanocarrier systems for dermal drug delivery can improve skin penetration, drug stability and reduce skin irritation by avoiding direct contact of the drug with the skin's surface [29]. Furthermore, they can improve the solubility of poorly water-soluble drugs, modify pharmacokinetics, increase drug half-life by reducing immunogenicity, improve bioavailability, and diminish drug metabolism [30].

Nanoparticles smaller than 40 nm might penetrate through the trans-epidermal and trans-follicular routes or aqueous pores, and their penetration is influenced by the furrows and wrinkles on the skin surface. Larger particles may favorably penetrate through the trans-follicular route (Figure 2) [31].

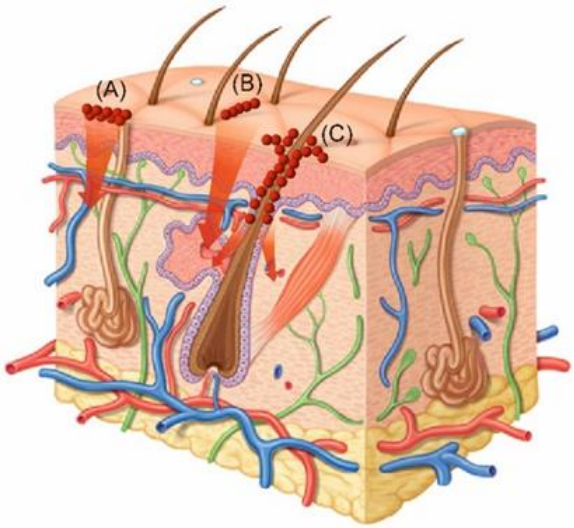

Fig. 2. Skin penetration pathways for nanoparticles: stratum corneum surface (A), furrows and wrinkles (B), hair follicles (C).

Among nanocarrier systems, liposomes are the most studied. Liposomes are bilayered phospholipid vesicles with an internal aqueous phase. They have a similar structure to biological membranes, with a typical size of 50-100 nm or even larger. They are usually prepared from well-tolerated components; their production is relatively easy on a large scale and they are capable of the simultaneous delivery of multiple drugs. Liposomes improve drug bioavailability, reduce systemic toxicity and increase the half-lives of drugs *in vivo* [32,33]. Furthermore, these carriers enable a more intense localization of the active agent in the layers of the skin [34].

Nanostructured lipid carriers (NLCs) are modern alternatives to liposomes with many advantages, such as better physical stability, low cost (no need for expensive phospholipids), the possibility of scale-up, the potential of epidermal targeting, follicular delivery, controlled drug delivery and photostability improvement of active pharmaceutical ingredients (APIs) [35]. NLCs are the second generation of lipid nanoparticles wherein solid lipids are partially substituted by liquid lipids. This structure allows the drug to be located in the liquid lipid, which predicts the better mobility of the drug, therefore improved stability and controlled drug release are achieved [36]. Additionally, the similarity of NLC forming lipids to physiological molecules makes these systems well-tolerated, biodegradable and nontoxic. Furthermore, lipid particles, when the particle size is less than 200 nm, form a thin layer on the skin surface, reducing the TEWL and increasing the hydration, thereby they facilitate the penetration of the incorporated drug and support the physiological conditions of the skin [37–39].

Lyotropic liquid crystal (LLC) systems are also becoming increasingly widespread because of their ability to be excellent drug carriers since they have a unique, skin-similarly structure and attractive physicochemical properties as they show a structure typical of fluids and the crystalline state of solids as well. They form gel-like phases with special internal structures, into which drugs can be loaded [40]. Their preparation is cost-effective and easy as they are usually formed with low energy input from water, oil phase and one or two surfactants and possibly cosurfactants in the definitive amounts of the components. Further advantages of these systems include easy storage, thermodynamic stability, sustained drug release, and similarity to colloid systems in living organisms. Furthermore, they can induce a considerable increase in the solubility of drugs by means of solubilization. LLC systems with a lamellar structure demonstrate the greatest similarity to the intercellular lipid membrane of the skin, so they are primarily recommended for the development of a dermal dosage form [41].

2.3.2. Active methods

Active penetration enhancement methods are often physical approaches that can cause cavitation, thermal, convective and mechanical effects in the skin to enhance drug delivery. Electroporation (EP), iontophoresis, ultrasound, laser radiation and photomechanical waves, microneedle-based devices, needleless injection, magnetophoresis, thermophoresis, radio frequency, suction ablation and skin abrasion are all current active techniques to improve penetration of drugs through the skin [42].

2.3.2.1. Electroporation

EP works with the application of short, high voltage pulses, which cause transitory structural perturbation in the lipid bilayer of the membranes, and thus EP can increase transdermal drug delivery by several orders of magnitude. This technique can be used to deliver drugs, DNA, antibodies, proteins, and fluorescent molecules to cells [43].

The short (10 μs to 10 ms duration) electric pulses form an electric field and when the transdermal voltage reaches 0.5-1 V, transient aqueous pathways appear [44]. This pore formation takes microseconds while the resealing of the membrane happens in the minute time range depending on the used electrical parameters and the temperature [45].

For the delivery of pulses to the skin, different types of electrodes specific to the application are used: plate, needle, needle-free microelectrode array and multi-electrode array electrodes. Depending on the electrode type, the delivery of the drugs can be controlled by the amplitude, the number and the duration of the electric pulses [43].

Electrochemotherapy (ECT) is a modern therapy to treat tumors located in the skin, which involves the local application of short, high voltage pulses to enhance the intracellular delivery of antitumor drugs (Figure 3) [46].

The first clinical use of EP for cancer treatment was in 1993 [47] and since then many studies have demonstrated the efficacy of this kind of treatment for various kinds of tumors, including head and neck squamous cell carcinoma, melanoma, basal cell carcinoma, adenocarcinoma and Kaposi's sarcoma [48–52]. In comparison with conventional chemotherapy, ECT causes little or no adverse effects [53]. With the standard treatments for melanoma metastases, the response rates range from 20 to 45 % with complete responses less than 5 % [53] in comparison with ECT, with which the complete response rates are between 60-70 % [46].

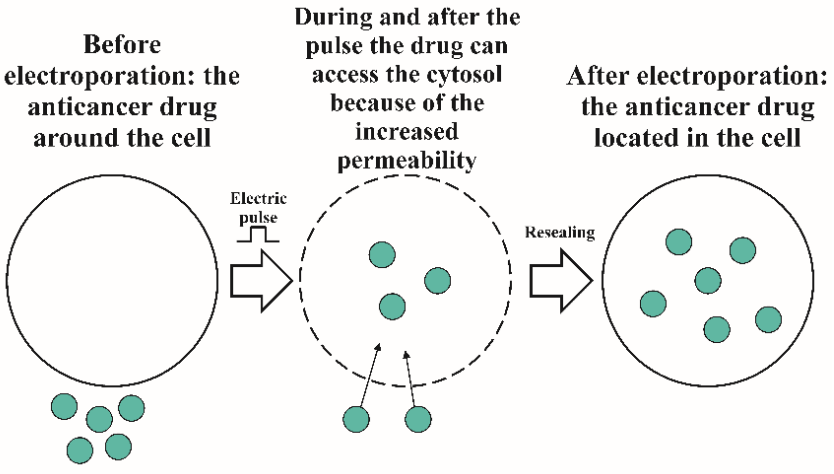

Fig. 3. Mechanism of action of ECT.

2.4. Formulation Design: Quality by Design method

Quality by Design (QbD) in pharmaceutics is a systematic, scientific, risk-based, holistic and proactive method that begins with determining objectives and puts emphasis on understanding product and processes control [29,54,55]. According to that, the quality needs to be designed into a drug formulation by understanding how material attributes of the APIs and the carrier system, and process parameters applied during the preparation affect the quality attributes of the formulation [56]. In the development of new pharmaceutical products, the application of the QbD approach results in a fast and improved optimization process by determining the quality target product profile (QTPP) and the critical quality attributes (CQA) [57–59]. Risk assessment (RA) is carried out to identify the potential hazards and parameters which possibly affect product quality [60].

The QbD based development starts with the definition of the target, namely the QTPP. According to the ICH Q8 guideline, QTPP is "a prospective summary of the quality characteristics of a drug product that ideally will be achieved to ensure the desired quality, taking into account safety and efficacy of the drug product" [67]. This step includes the preliminary definition of various essential parameters, such as the mode of administration, strength, dosage form, therapeutic area and aim, release profile, etc. QTPPs are determined to ensure the quality, safety and efficacy of the product.

The second step is to estimate the factors that guarantee the expected quality of the formulation (QTPPs). These are defined as CQAs: "physical, chemical, biological, or microbiological properties or characteristics that should be within an appropriate limit, range, or distribution to ensure the desired product quality" [67]. For example, quality attributes like size, charge, shape, type of surface modification, and biocompatibility have to be refined to provide the required therapeutic effect. The CQAs are usually defined properties, such as physical attributes, viscosity, homogeneity of the semisolid dosage form. The next step is to determine the critical material attributes (CMAs) and critical process parameters (CPPs), "process parameters whose variability has an impact on a CQA and therefore should be monitored or controlled to ensure the process produces the desired quality" [67]. All of them are based on the developers' prior practical and literature knowledge and experience [61].

RA is also a key-element of QbD, which is "a systematic process of organizing information to support a risk decision. It consists of the identification of hazards and the analysis and evaluation of risks associated with exposure to those hazards" [62]. Performing this step before the development of a product can help the researcher to decide which studies need to be conducted, thus RA is essential to save time and research process. It is done to

identify which attributes have a low, medium and high impact on the final formulation, thus it helps in prioritizing process parameters. With the help of this method, critical and non-critical variables can be defined to establish a control strategy for in process and final testing (Figure 4).

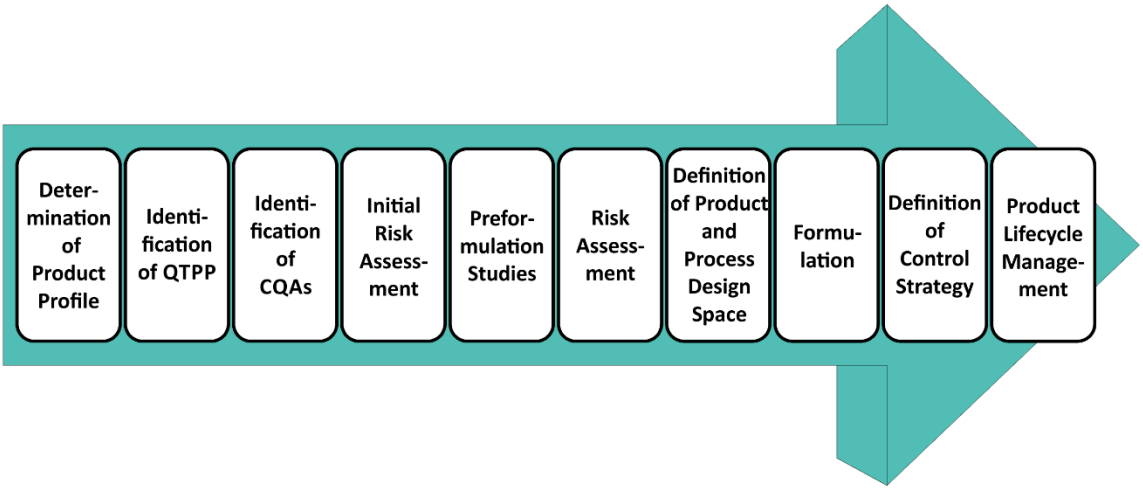

Fig. 4. Flowchart of QbD approach in formulation development.

2.5. Testing of dermal products: *in vitro* skin models

For utilizing and understanding the potential of transdermal route completely, the optimization of drug delivery systems is indispensable. Most of the current developments rely on the use of animal or human skin. However, the limited availability of human skin and the increasing restrictions in connection with animal testing are encouraging the development of suitable artificial skin models [63]. *In vitro* skin models have advantages, such as reproducibility, relatively low cost, easy storage, uncomplicated handling, and they offer a possibility for rapid screening and faster optimization of dermal formulations. Furthermore, their composition can be easily modified, which allows studying the relationship between certain pathological conditions and the barrier function. However, the limitations of these models need to be considered.

In vitro skin models can be classified as non-lipid-based, lipid-based models and reconstructed human skin equivalents. Among non-lipid-based models, silicon-based membranes are the most widespread [64]. They can be used for screening the effects of different vehicles and assessing their impact on the overall mechanisms of drug transport across human skin, however, they have limitations. A novel non-lipid-based attempt for modeling skin is the Strat-M™, which contains multiple layers of polyether sulfone creating the morphology similar to human skin [65]. Among lipid-based models like ceramide-derived parallel artificial membrane permeability assay (PAMPA) [66], phospholipid vesicle-based

permeation assay (PVPA) [67] and SC substitute models [68] are the most important. Reconstructed human skin equivalents are tissue culture-based human skin models, which have become commercially available in the past ten years. They are suitable for testing phototoxicity, corrosivity and irritancy, as well as for drug permeability studies [69]. These models are appropriate for rapid screening and faster optimization of dermal formulations, but their limitations need to be taken into consideration [63].

SC lipid liposomes (SCLLs) are composed of a lipid mixture approximating the composition of the SC: ceramides (40%), cholesterol (25%), cholesteryl sulfate (10%) and free fatty acids (25%). These lipid compositions are capable of forming unilamellar bilayers at physiological pH, and they were shown to be really stable [70,71]. These systems can be applied as *in vitro* models for screening agents of pharmaceutical or cosmetic interest, enabling the evaluation of their interactions with the permeability barrier [71].

3. EXPERIMENTAL AIMS

The aim of my Ph.D. work was to investigate promising dermal therapies, including novel drug delivery systems, active and passive penetration enhancement methods, and the opportunity to model the skin during the formulation development process.

1. In the first part of my work, liposomal skin modeling systems were prepared and investigated. The aim of this part was to evaluate the feasibility of *in vitro* model systems for predicting the effects of penetration enhancers on the skin. Two modern chemical penetration enhancers, Kolliphor RH40 and Transcutol, were investigated. Their enhancement effect was also studied by *ex vivo* penetration experiments. The correlation between *in vitro* and *ex vivo* results was calculated, thus the applicability of liposomal skin models for evaluating the effect of chemical penetration enhancers was determined.
2. In the second part, a topical betulinic acid-containing anticancer formulation was developed, and its penetration through the skin was followed-up by Raman spectroscopic mapping. The effect of electroporation on the penetration of betulinic acid was also determined. The aim was to develop a potential non-invasive, topical therapy for cutaneous melanoma.
3. In the third part, different lidocaine-containing carrier systems were developed and investigated: the drug was incorporated in hydrogel, oleogel, liposome, NLC and LLC. For the determination of the encapsulation efficiency of liposomes, DSC was used as a novel

approach. For the optimization of the other carrier systems and for the selection of the appropriate examination method, the Quality by Design method was applied.

The following aims were set:

- to incorporate the salt and base form of lidocaine in conventional and novel drug delivery systems;
- to characterize the vehicles in terms of:
  - particle size (dynamic light scattering method),
  - zeta-potential (electrophoretic mobility method),
  - encapsulation efficiency (ultracentrifugation, DSC),
  - drug-carrier interactions (FT-IR and Raman spectroscopy);
- to apply the Quality by Design method for determining the most critical characteristics influencing the quality of the formulation which have to be examined during the development process;
- to examine the release and skin penetration of lidocaine incorporated in different carrier systems *in vitro* and *ex vivo* by a vertical Franz diffusion cell;
- to investigate the influence of the carrier systems on the physiological skin conditions *in vivo* (skin hydration and TEWL);
- to follow-up drug penetration into skin cross-section by Raman spectroscopic mapping.

My Ph.D. work plan is summarized in Figure 5.

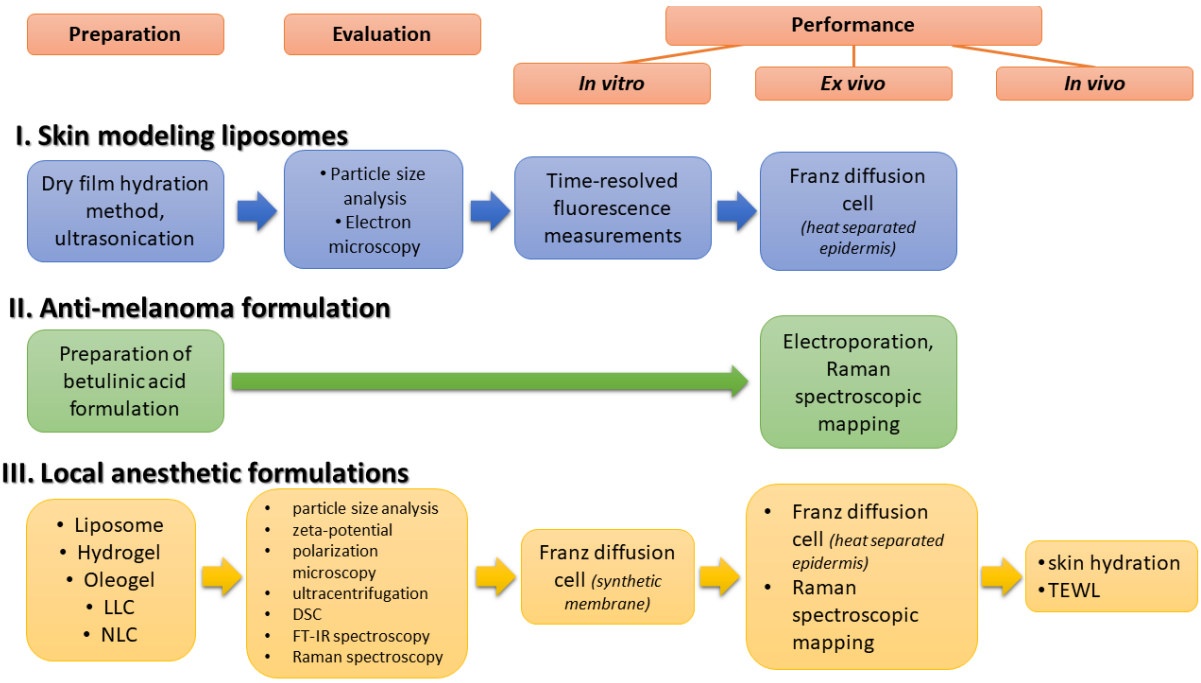

Fig. 5. The overall scheme of the Ph.D. work.

4. MATERIALS AND METHODS

4.1. Materials

4.1.1. Skin modeling liposomes

The preparation of SCLLs followed the method described by Wertz et al. [71]. Individual lipids (ceramide III and VI, Evonik Industries, Essen, Germany; cholesterol, Hungaropharma Ltd., Budapest, Hungary; palmitic acid, Mosselman s.a., Ghlin, Belgium; and cholesterol sulfate, Sigma-Aldrich, Saint Louis, Missouri, USA) were dissolved in chloroform-methanol (2:1 by volume, Carl Roth GmbH&Co. KG, Karlsruhe, Germany) and appropriate volumes were combined to obtain the corresponding mixture (ceramides: cholesterol: palmitic acid: cholesterol sulfate= 4: 2.5: 2.5: 1, wt%). The lipid mixture was then placed in a culture tube, and the solvent was removed with a stream of nitrogen (Christ RVC 2-18 Vacuum Concentrator, Martin Christ Gefriertrocknungsanlagen GmbH, Osterode am Harz, Germany) and then under high vacuum at room temperature. Aqueous dispersions of each lipid mixture were prepared by suspension in buffer containing 20 mM HEPES (4-(2-hydroxyethyl)-1-piperazineethanesulfonic acid, Carl Roth GmbH&Co. KG, Karlsruhe, Germany), 120 mM NaCl (Carl Roth GmbH & Co. KG, Karlsruhe, Germany), 0.8 mM EDTA (Sigma-Aldrich, Saint Louis, Missouri, USA) at pH 8. For calcein efflux measurements the buffer contained 70 mM calcein dye (Sigma-Aldrich, Saint Louis, Missouri, USA) instead of NaCl. The final lipid concentration was 5 mg mL^{-1}. The lipids were left to hydrate for 30 min with occasional shaking. The suspensions were then sonicated in a bath sonicator at 80°C (temperature slightly higher than the phase transition temperature of lipid mixture) for about 1 h until the suspensions became clear. The preparations were then annealed at the same temperature for 30 min. Liposomal formulations were stored at 4°C and used within 1 day.

4.1.2. Betulinic acid-containing formulation

Betulinic acid (Cayman Chemical Company, Ann Arbor, USA) was partly dissolved in the mixture of 2-propanol (Merck Ltd., Budapest, Hungary), Transcutol, Labrasol (Azelis Hungary Ltd., Budapest, Hungary) and isopropyl myristate (Merck Ltd., Budapest, Hungary). PEG 4000 (Merck Ltd., Budapest, Hungary) was melted and homogenized with this suspension. The ointment was stirred until cooling.

4.1.3. Lidocaine-containing formulations

4.1.3.1. Hydrogel

Conventional hydrogel was prepared from 5 wt% LID hydrochloride (Hungaropharma Ltd., Budapest, Hungary) dissolved in the mixture of purified water, ethanol and macrogol 400

(Hungaropharma Ltd., Budapest, Hungary), and 3 wt% Methocel K4M (Colorcon, Budapest, Hungary) was added to this solution as the gelling agent.

4.1.3.2. Oleogel

Mygliol 812N (Sasol GmbH, Hamburg, Germany) and Kolliphor RH40 (as a penetration enhancer, BASF SE Chemtrade GmbH, Ludwigshafen, Germany) mixture was heated to 60°C and 5 wt% LID base (Hungaropharma Ltd., Budapest, Hungary) was dissolved in this mixture. 5 wt% Aerosil 200 (Sigma-Aldrich, Saint Louis, Missouri, USA) was added to prepare gels.

4.1.3.3. LLC

Isopropyl myristate and Kolliphor RH40 1:4 mixture was heated (60°C) and homogenized with a magnetic stirrer, 5 wt% LID base was dissolved and 10 wt% water was then added to the lipid phase drop by drop under stirring.

4.1.3.4. NLC

The solid lipid Apifil (PEG-8 Beeswax, Gattefossé, St. Priest, France) was melted at 80°C, Mygliol 812N and LID base were added under moderate stirring. Under the same conditions, the water phase was prepared with surfactant (Cremophor RH60, BASF SE Chemtrade GmbH, Ludwigshafen, Germany). Then the water phase was added to the lipid phase and put under high shear homogenizer for 1 min (8000 rpm). The obtained pre-emulsion was ultrasonified using a Hielscher UP200S compact ultrasonic homogenizer (Hielscher Ultrasonics GmbH, Germany) for one cycle, 70% amplitude, 10 min. In the end, the sample was cooled down in an ice bath to get the NLC dispersion. Then, a gel was formed (at room temperature) with glycerin and Methocel K4M and the NLC dispersion was added to reach a final 5 wt% LID concentration.

4.1.3.5. Liposome

LID-containing liposomes were prepared by dry film hydration method [72]. Stock solutions were prepared of DMPC (1,2-dimyristoyl-sn-glycero-3-phosphocholine, Avanti Polar Lipids, Alabaster, Alabama) and LID base with chloroform. Aliquots were added to individual vials to reach 5 mg mL^{-1} lipid and 1-2-3-4-10 wt% LID. These solutions were dried under vacuum (30°C, 1.5 h, 1500 rpm, Christ RVC 2-18 Vacuum Concentrator, Martin Christ Gefriertrocknungsanlagen GmbH, Osterode am Harz, Germany). The lipid film was then placed in a vacuum desiccator overnight, to ensure the complete removal of the solvent. The hydration of the film was done with 1 mL HEPES buffer (20 mM, containing 154 mM NaCl, pH 7.4) at room temperature, alternating with vortex agitation for 5 min. Liposomal formulations were stored at 4°C and used within 1 week.

4.2. Methods

4.2.1. *In vitro* methods

4.2.1.1. Particle size and zeta potential measurements

Measurements for liposomes and NLC were taken with a Malvern Nano ZS device based on dynamic light scattering. Samples were thermostated to 25°C. Measurements were taken in standard disposable cuvettes using Malvern's dip cell, in triplicate. To ensure the validity of the data, a zeta standard was measured every 30 min. Polydispersity index was also evaluated to define the homogeneity of the dispersion.

4.2.1.2. Ultracentrifugation

The encapsulation efficiency (EE%) of LID-containing liposomes was determined using ultracentrifugation method combined with UV/Vis spectrophotometry. About 1 g of each liposome preparation was placed into Beckman polycarbonate centrifuge tubes and diluted to 1.5 mL with HEPES buffer. The samples were centrifuged in a Beckman Coulter Optima XE-90 Ultracentrifuge (Beckman Coulter Inc., Brea, CA, USA) for 3 h at 35000 rpm at 4°C. The supernatant was removed, leaving the pellet containing the liposomes at the bottom of the tubes. Then a washing step was performed: 1.5 mL of the HEPES buffer was added to the pellet and the centrifugation process was repeated. After that, the supernatant was removed again. Both the supernatant ("indirect method") and the pellet (dissolved in 1 mL ethanol "direct method") were measured with UV spectrometer at 262 nm to determine LID concentration.

4.2.1.3. Differential scanning calorimetry measurements

Differential scanning calorimetry (DSC) measurements of LID-containing liposomes were performed using a MicroCal VP-DSC device (MicroCal Inc., Northampton, USA). As a reference, 20 mM HEPES buffer solution was used. Before the calorimetric experiments, the solutions were degassed and then filled into the sample cell (0.4988 mL). A heating rate of 1°C min^{-1} in the 5-80°C range was applied. Origin 7.0 software was used to subtract the baselines from the curves and to convert the raw data into data of molar heat capacity.

DSC method can provide information about the drug-lipid interactions, size, partition coefficient and encapsulation efficiency with one measurement [73]. In my experiments, we focused on the comparison of the generally used ultracentrifugation method and DSC for the evaluation of encapsulation efficiency. The principle of using DSC for this approach is based on the reduction of temperature of the main phase transition depending on the partitioning of LID between the fluid or in the gel phase of the lipid [74].

If the drug mixes ideally with the fluid phase of the membrane but it is completely excluded from the gel, the difference between the actual phase transition temperature (T) and the temperature of the main phase transition of pure lipid (T_0) can be written as ($\Delta T_m = T_0 - T$):

$$\Delta Tm(X) = -\frac{RT^2}{\Delta H} X_d^b \tag{1}$$

where R is the ideal gas constant (1.9858775 cal K^{-1} mol^{-1}), ΔH is the enthalpy of the main phase transition, and X_d^b is the molar fraction of the drug bounded in the liposome [29]. So, the shift of the melting temperature is independent from the special properties of the drug (as long as the ΔH of melting is not strongly affected) and proportional to its mole fraction in the membrane [75].

Knowing the mass of the liposome measured, units can be converted from mole fraction to concentration [76]:

$$c_d^b = c_{lipid} \frac{X_d^b}{1 - X_d^b} \tag{2}$$

where c_d^b is the concentration of the bounded drug and c_{lipid} is the lipid concentration.

From these values, the encapsulation efficiency can be calculated:

$$EE\% = \frac{c_d^b}{c_d^{total}} \approx \frac{X_d^b}{X_d^{total}} \tag{3}$$

To characterize a formulation, it is also useful to determine its membrane-water partitioning properties because lipophilicity plays an important role in biological activity. The direct calculation of solute partitioning into bilayers can also be performed by DSC [76]. According to previous empirical evidence, the free drug concentration is proportional to the mole ratio of drug to lipid in the membrane (R), so the mole ratio partition coefficient (K_R) can be calculated [30, 32, 33]:

$$K_R = \frac{R}{c_d^{free}} = \frac{c_d^b}{c_d^{free} c_{lipid}} \tag{4}$$

where c_d^{total} is the total drug concentration, c_d^{free} is the unentrapped drug concentration and X_d^{total} is the maximum bounded drug fraction.

4.2.1.4. Polarization microscopic analysis

The LLC samples were investigated under polarized light microscopy in order to study the texture of the lamellar phases. A small quantity of the sample was placed on a clean glass slide and observed under crossed polars using a magnification of 200×.

4.2.1.5. Fourier transform infrared spectroscopic analysis of NLC

The Fourier transform infrared spectroscopy (FT-IR) spectra of LID-NLC were recorded with an Avatar 330 FT-IR spectrometer (Thermo Fisher Scientific Inc., Waltham, MA, USA) equipped with a horizontal ATR crystal (ZnSe, 45°), between 4000 and 400 cm^{-1}, with 128 scans, at an optical resolution of 4 cm^{-1}. For the spectral analysis Thermo Scientific GRAMS/AI Suite software (Thermo Fisher Scientific Inc., Waltham, MA, USA) was used.

4.2.1.6. Raman spectroscopic measurements of lidocaine-containing formulations

The Raman spectra of the formulations were acquired with a Thermo Fisher DXR Dispersive Raman Spectrometer (Thermo Fisher Scientific Inc., Waltham, MA, USA) equipped with a CCD camera and a diode laser operating at 532 nm. The spectra of the components, LID-free and LID-containing samples were acquired with an exposure time of 6 s, 24 scans, including cosmic ray and fluorescence corrections. Measurements were carried out with a laser power of 10 mW at a slit width of 25 μm.

4.2.1.7. Calcein efflux and lifetime-based fluorescence leakage assay

To determine the disruption effect brought about by CPEs, the degree of calcein efflux from SCLLs was examined. Calcein leakage assay is based on the fact that the calcein entrapped in liposomes expresses only slight fluorescence due to self-quenching or co-entrapment of a quencher, but when it is released from the liposomes and attenuates, it shows fluorescence. The efflux is defined as the fraction of previously entrapped calcein that was released within a defined time point after exposure to the permeabilizer [19].

Calcein efflux (E) was calculated according to the following equation [17]:

$$E = \frac{(B_F - B_{F0})}{(B_F - B_{F0} + Q_{stat}\ B_E)} \quad (5)$$

where B is the pre-exponential factor (proportional to concentrations of free and entrapped dye). B_{F0} corresponds to the free dye at the beginning of the measurement (this corrects for incomplete dye removal on the column), B_F to free dye concentration at certain time points and B_E to the entrapped calcein concentration. Q_{stat} is the static quenching factor which considers that some entrapped dye might be ‘invisible’ due to dimerization. We used Q_{stat}=1.2 based on the literature [17].

Before the fluorescence measurements, vesicles were separated from the unencapsulated fluorescent dye on a PD-10 desalting column (GE Healthcare, Little Chalfont, UK) using HEPES buffer (20 mM HEPES, 120 mM NaCl, 0.8 mM EDTA, pH 8) as the mobile phase. 5 µl aliquots of these vesicles were incubated with different concentrations of CPEs, at room temperature on a gently rotating shaker and efflux measurements were performed after 1, 10, 30 min, 1, 2, 3 h. The samples were placed in a Horiba Jobin Yvon (Horiba Ltd., Edison, New Jersey, USA) Fluorolog 3 system equipped with a 467 nm laser diode pulsing at 1 MHz for excitation. The decay curve was recorded at a wavelength of 515 nm (bandwidth 2 nm) for 25 s using time-correlated single photon counting. We used Horiba DAS6 software to fit decay curves biexponentially by deconvoluting them with the instrument response function as measured with a scattering LUDOX® solution.

4.2.2. Drug diffusion and penetration investigations *in vitro* and *ex vivo*

4.2.2.1. Preparation of heat-separated epidermis

Excised human skin was obtained from a Caucasian female patient who underwent abdominal plastic surgery, with the approval of the Ethical Committee of the University of Szeged, Albert Szent-Györgyi Clinical Centre (Human Investigation Review Board license number: 83/2008.). For the separation of the epidermis, the heat separation technique was applied [77]. The obtained epidermal membrane was applied onto the surface of PBS (phosphate buffered saline, pH 7.4) for at least 20 min and then set on a supporting mixed cellulose ester membrane (pore diameter 0.45 µm, Porafil, Machenerey-Nagel, Düren, Germany, and Pall Life Sciences, Washington, NY, USA) for the *ex vivo* measurements.

4.2.2.2. Franz diffusion cell method

In vitro release and *ex vivo* penetration were measured using a vertical Franz diffusion cell system (Hanson Research, Chatsworth, CA, USA) in a six-unit assembly (effective permeation area 1.676 cm^2) for 24 h at 32± 0.5°C. The donor phase was either 0.30–0.40 g of the appropriate LID-containing formulation or 1 mL caffeine solution, which was placed on a mixed cellulose ester membrane (Porafil, Machenerey-Nagel, Düren, Germany, and Pall Life Sciences, Washington, NY, USA) itself (*in vitro*), or in case of *ex vivo* measurements the epidermis was supported with a Porafil membrane filter. PBS pH 7.4 was used as the acceptor medium and it was stirred at 450 rpm throughout the experiment. At selected time intervals, samples of 0.8 mL were taken from the acceptor phase by the autosampler and replaced with an equal volume of fresh receiver medium. The amount of permeated drug was measured using a Unicam Heλios Thermospectronic UV/Vis spectrophotometer (Unicam, Thermo

Fisher Scientific Inc., Waltham, MA, USA) in case of LID at 262 nm or high-performance liquid chromatography (HPLC) in case of caffeine.

4.2.2.3. High-performance liquid chromatography

The HPLC analysis of caffeine was performed with a Shimadzu Nexera X2 UHPLC system. The system control and data acquisition were performed with Shimadzu LabSolutions software package. The chromatographic separation was achieved by Phenomenex Kinetex C18 column with 2.6 μm particle size (150×4.6 mm I.D.). The column temperature was maintained at 25°C. The separations were carried out in isocratic mode. The mobile phase was a mixture of pure HPLC grade water and methanol in the ratio of 75:25, the eluent's flow rate was 1.0 mL/min. For the detection of caffeine, PDA detector was used. The wavelength of detection was 272 nm and the detector cell temperature was adjusted to 40°C. The sample tray holder's temperature was 25°C, the injected volumes of the samples were 5 μL. The analysis time was 7 min, the retention time of caffeine was ~5.1 min

4.2.2.4. Penetration parameters

The penetration was calculated in terms of the mean cumulative amount permeated through the membrane, taking the diffusion area into account. The results were plotted as a function of time. The steady-state flux (J) was calculated from the slope of the linear regression versus $t^{1/2}$ and expressed in $\mu g\ cm^{-2}\ h^{-1}$.

4.2.3. Raman mapping

4.2.3.1. Preparation of skin cross-sections

Excised human skin was obtained from a Caucasian female patient who underwent abdominal plastic surgery, with the approval of the Ethical Committee of the University of Szeged, Albert Szent-Györgyi Clinical Centre (Human Investigation Review Board license number: 83/2008). The skin surface was gently wiped off with cotton swabs soaked in 10% ethanolic solution and stored at -21°C for no more than 6 months, prior to usage. For penetration experiments, the skin was defrosted and placed on a filter paper soaked in physiologic saline solution with the SC side up. Then, formulations were placed on the skin surface in a silicon ring with a surface area of 0.63 cm^2 and 1 mm height. The time of diffusion was 6 h, incubation was carried out at 34-36°C. Full-thickness skin samples were excised from the treated areas, embedded in Cryomatrix resin (Thermo Fisher Scientific Inc., Waltham, MA, USA) and cryosections of 10 μm thickness were made. For Raman mapping, the microtomed skin samples were placed on an aluminum surface with the SC towards the top of the plate.

4.2.3.2. Raman spectroscopic measurements of skin cross-sections

The localization of LID and BA in the skin samples was investigated by Raman mapping. Measurements were performed with a Thermo Fisher DXR Dispersive Raman Spectrometer (Thermo Fisher Scientific Inc., Waltham, MA, USA) equipped with a CCD camera and a diode laser. For these measurements, the excitation source was 780 nm laser light, which is the most effective source for investigating biological samples, providing the sufficient energy for the vibrations of protein alternatives in the skin. The laser power focused on the sample was 24 mW. Measurements were recorded using a 50x objective. The acquisition time of each spectrum was 12 times 2 s and the spectrograph aperture was adjusted to 25 μm slit, providing suitable penetration of the light into the skin sample. The mapping was performed using a point-by-point mode, applying a step size of 50 μm perpendicular and parallel to the SC. Data acquisition and analysis were accomplished using OMNIC™ 8.2 for Dispersive Raman software package (Thermo Fisher Scientific Inc., Waltham, MA, USA).

4.2.4. *In vivo* experiments

4.2.4.1. Electroporation experiments

Six-month-old female SKH-1 hairless mice were housed in a thermoneutral environment in plastic cages with a 12 h light-dark cycle. They had availability to standard laboratory chow and drink water *ad libitum*. All experiments were in full accordance with the NIH guidelines and the interventions were approved in advance by the Ethical Committee for the Protection of Animals in Scientific Research at the University of Szeged (license number: V./145/2013).

Prior to the treatments, the animals were anesthetized with a mixture of ketamine (90 mg (kg bodyweight)$^{-1}$) and xylazine (25 mg (kg bodyweight)$^{-1}$) administered intraperitoneally. At the end of the experiments, the mice were euthanized with an overdose of ketamine (300 mg kg^{-1}).

The mice involved in the study were divided into 4 groups as follows (2 mice were randomly assigned to each group):

- Group A: mice treated with dermally applied BA ointment for 30 min (conventional treatment)
- Group B: mice treated with BA ointment and EP at 900 V for 1 min
- Group C: mice treated with BA ointment and EP at 900 V for 2 min
- Group D: mice treated with BA ointment and EP at 900 V for 6 min

For the conventional treatment (Group A), 0.1 grams of the ointment was deposited on the dorsal skin surface of hairless mouse, left for 30 min for penetration, and after the diffusion

period the skin surface was cleaned with a dry cotton swab. For the EP processes (Group B, C, D) also 0.1 grams of the ointment was deposited on the skin, the treatment was performed with the headpiece, and then the skin was cleaned as mentioned before.

A Mezoforte Duo Mez 120905-D instrument (Dr. Derm Equipment Ltd., Budapest, Hungary) was used to generate the electric pulses for the skin EP. The operation of this device is based on a pulsed electromagnetic field generated by an amplitude-modulated sine wave radiofrequency current. The polypropylene-covered treatment headpiece contains a plate electrode 25 mm in diameter indirectly contacting with the treated surface. Modulation involves 900 V pulses 5 ms in duration, followed by a 20 ms break. Drug transport by means of skin EP can be determined by different treatment times (1, 2 or 6 min).

For Raman measurements, at the end of the observation period, the animals were sacrificed (as described above) and full-thickness skin samples were excised from the treated areas. The samples were embedded in Cryomatrix resin (Thermo Fisher Scientific Inc., Waltham, MA, USA) and cryosections of 6 μm were made.

4.2.4.2. Skin hydration and TEWL measurements

3-4-month-old male SKH-1 hairless mice were kept and anesthetized as mentioned before. For the treatment, 0.2 g of each formulation was deposited on the dorsal skin surface of hairless mice, left for 30 min for penetration, and after the diffusion period the skin surface was cleaned with a dry cotton swab. Skin hydration was measured using a Corneometer CM 825 and TEWL was evaluated with Tewameter TM 300, both connected to a Multi Probe Adapter MPA 5 (Courage+Khazaka Electronic GmbH, Germany), 30, 90 and 150 min after the application. The results are given in percentage compared to the levels before treatment.

4.2.5. Statistical analysis

One-way ANOVA followed by the Bonferroni test was used to determine the statistical differences between the results by using GraphPad Prism software (GraphPad Software Inc., La Jolla, CA, USA). Differences were regarded as significant if p\0.05*, p\0.01** and p\0.001***.

5. RESULTS AND DISCUSSION

5.1. Investigation of SCLL liposomes as potential models for skin

5.1.1. SCLL characteristics: particle size and polydispersity index

The particle size and polydispersity index (PDI) of SCLLs with and without calcein are represented in Table 1. The electron microscopic images revealed that most of the particles were unilamellar.

Table 1. Particle size and PDI of "blank" and calcein-loaded SCLLs.

	Z-ave (nm)	PDI
SCLL	135.23 ±0.06	0.220±0.02
Calcein-loaded SCLL	137.35±0.07	0.228±0.02

5.1.2. Calcein efflux and lifetime-based fluorescence leakage assay

The effect of different concentrations of Kolliphor RH40 and Transcutol was tested on the disruption of SCLLs applying calcein leakage assay.

First, the correlation between the enhancer concentration and the efflux was investigated for 3 h (Figure 6). Both Kolliphor RH40 and Transcutol promoted calcein efflux from SCLLs in a concentration-dependent manner. However, from Transcutol, much higher concentration was needed to achieve the same efflux value. The efflux curve for Transcutol reached a plateau value after about 1 h, while the calcein efflux caused by Kolliphor RH40 increased even after 2 h. For longer waiting times, there was only a slight further increase with a much slower rate.

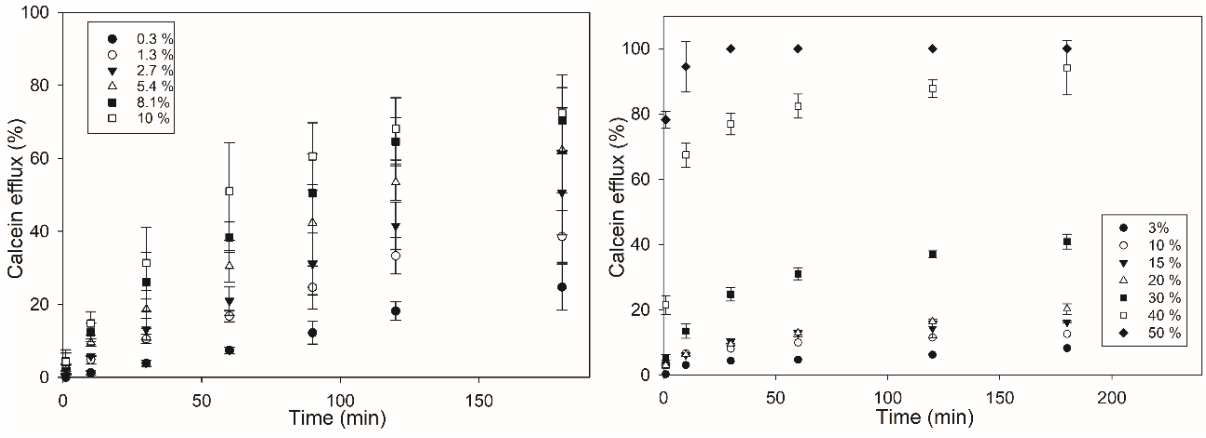

(A) **(B)**

Fig. 6. Efflux from SCLLs induced by Kolliphor RH40 (A) and Transcutol (B) as a function of incubation time. The concentration of the CPEs are indicated in the plot.

We investigated the relationship between CPE concentration and calcein efflux after 1 h. The concentration profiles of the efflux were different for the two investigated CPEs. Kolliphor RH40 showed a linear relationship between calcein efflux and concentration, while in case of Transcutol, a concave downward profile was observable, which indicated a limit for the disruption of SCLLs (Figure 7).

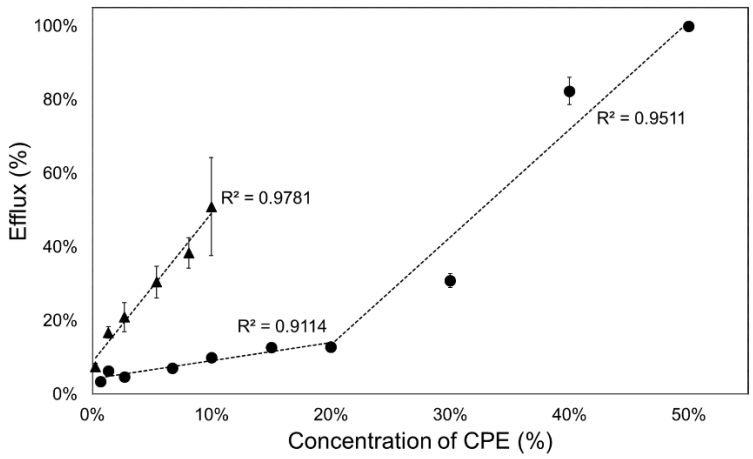

Fig. 7. Calcein efflux from SCLLs after 1 h of incubation as a function of CPE concentration (▲: Kolliphor RH40, ●: Transcutol).

However, these results do not give detailed information about the characteristics of vesicle disruption. The efflux can result mainly from two mechanisms: (i) all-or-none, when only some vesicles are disrupted (and releasing all entrapped dye) while others remain undamaged or (ii) graded, when all vesicles release a certain fraction of their content.

The fluorescence lifetime measurement method published by Patel et al. [78] can distinguish between these two mechanisms by plotting calcein efflux versus the lifetime of entrapped dye (τ_E). Ideally, homogeneously graded leakage points of the above-mentioned graph should lie on the diagonal (efflux E couples directly with the entrapped calcein concentration: the more has leaked out, the less is left behind, which correlates with τ_E). The right-shift of E(τ_E) from the diagonal is a measure for the heterogeneity of graded leakage. All-or-none leakage increases E but does not affect τ_E since the entrapped calcein concentration in the non-leaky vesicles remains 0.4 ns and the empty vesicles do not contribute to τ_E at all, thus E(τ_E) should follow a vertical line at τ_E 0.4.

Vesicles incubated with Kolliphor RH40 showed all-or-none leakage mechanism until a certain point around 60% efflux, then efflux became graded. The efflux increased with increasing concentration of Kolliphor RH40 and with time (Figure 8A).

Transcutol caused graded leakage of the vesicles, which is in agreement with the previous results: calcein efflux is not promoted at lower concentrations, a certain concentration of Transcutol is needed to increase the efflux to a great extent (Figure 8B). This finding is in agreement with a previous study [24]. Transcutol is reported to interact with the aqueous domain of the lipid bilayer which increase the solubility of drugs in the skin. According to Moghadam et al., Transcutol caused only a slight disordering effect within the SC membrane. They also proved the superior enhancer effect of Kolliphor RH40 [27].

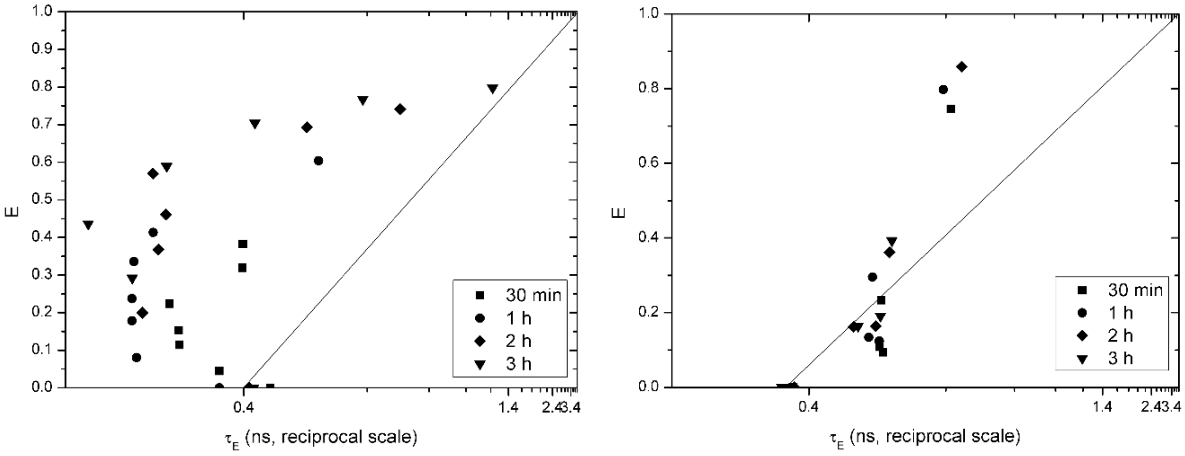

Fig. 8. Calcein efflux as a function of the entrapped fluorescence lifetime on a reciprocal scale brought on by Kolliphor RH40 (A) and Transcutol (B).

5.1.3. Effect of Kolliphor RH40 on the *ex vivo* penetration of caffeine

Caffeine was selected as a hydrophilic model drug to determine the penetration enhancer effect of different concentrations of Kolliphor RH40 on human epidermis *ex vivo*. Figure 9 shows the cumulative amounts of caffeine penetrated through heat separated epidermis (HSE) over 24 hours.

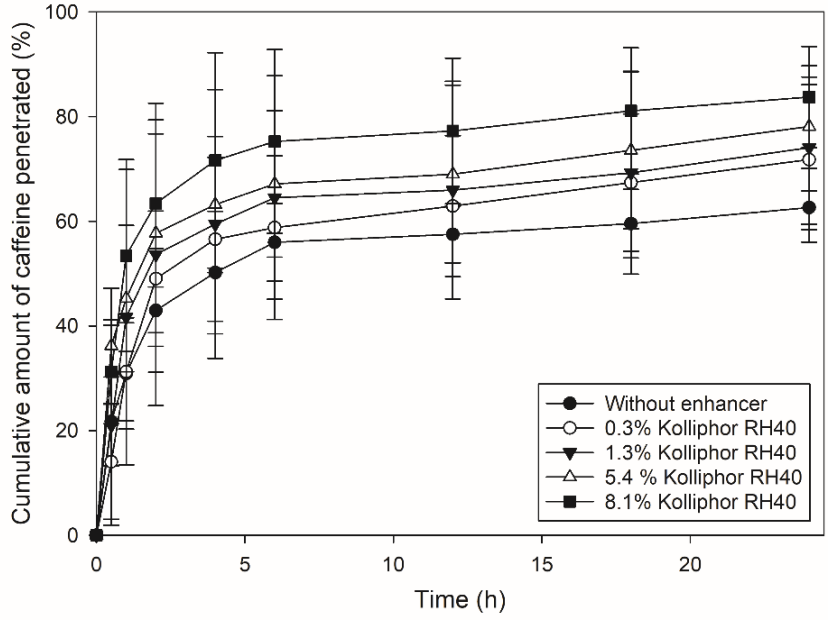

Fig. 9. Cumulative amount of caffeine penetrated through HSE after application of different concentrations of Kolliphor RH40.

It can be stated that the *ex vivo* penetration of caffeine was strongly dependent on the concentration of Kolliphor RH40: with an increasing concentration of the penetration enhancer, the skin penetration of caffeine also increased. The highest concentration of Kolliphor RH40 applied was 8.1% and it caused 21% increase in the penetration of caffeine compared to the blank caffeine solution after 24 h.

5.1.4. Relationship between calcein leakage and *ex vivo* skin penetration

Calcein leakage assay performed with SCLLs was applied as an *in vitro* model to investigate the enhancer effect of CPEs. We attempted to evaluate the correlation between the *in vitro* SCLL-based data and the *ex vivo* results gained by conventional penetration experiments. For this reason, we evaluated the change in the penetrated amount of caffeine compared to the blank formulation and the increase in efflux *in vitro* compared to SCLLs without enhancer after 1 and 2 h.

Figure 10 shows the relationship between the increase in the cumulative permeated amount of caffeine compared to blank solution and calcein leakage from SCLLs. The correlation coefficient of this relationship was 0.915 after 1 h and 0.954 after 2 h. According to the results, Kolliphor RH40 affected SCLL disruption more markedly than the skin permeation of caffeine, which could be the result of different lipid-enhancer ratios in these cases. Our results suggest that SCLLs could be promising *in vitro* approaches for screening the effects and effective concentrations of chemical penetration enhancers as we found a good correlation between SCLL-based experiments and the skin penetration study.

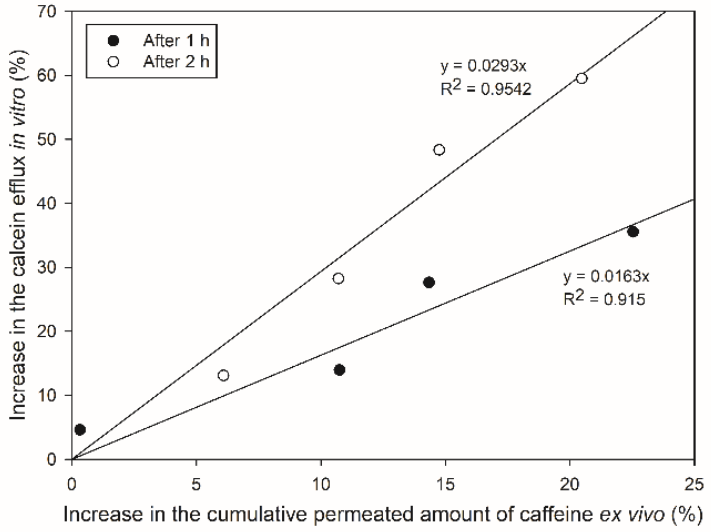

Fig. 10. Relationship between calcein leakage and increase in the caffeine permeated compared to blank formulation after 1 and 2 hours.

5.2. Examination of the penetration of the betulinic acid-containing formulation

The effect of EP on the penetration of BA ointment was studied by Raman scattering experiments. Raman chemical mapping was used to confirm the localization of BA in various skin depths.

5.2.1. Raman spectral features of the formulation

The first step of our study consisted of establishing the spectral features for BA and for the BA containing ointment (Table 2).

Table 2. Assignment of BA vibrations.

Raman shift (cm^{-1})			
BA in solid state	**BA ointment**	**Based on literature[62]**	**Assignment**
2943	2940	2944 vvs	C-H un. stretch
2871	2876	2875 vs	C-H sat. stretch
1646	-	1646 s	C=O stretch
1449	1449	1451 vs	CH_3 bend
-	1394	1400 m	C-CH_3 bend
-	1359	1356 m-w	COO-stretch
-	-	1320 m	CH_2 bend
1232	1231	1232 m	mixed, C-H bend, C-C bend, C-O bend
1198	1198	1195 vs	mixed, C-H bend, C-C bend, C-O bend
1130	1128	1157, 1130 m	mixed, C-H bend, C-C bend, C-O bend
-	1088	1107,1088 m	mixed, C-H bend, C-C bend, C-O bend
-	1046	1043 sh	mixed, C-H bend, C-C bend, C-O bend
983	-	982 m	mixed, C-H bend, C-C bend, C-O bend
945	-	942 m	mixed, C-H bend, C-C bend, C-O bend
916	-	919 m	mixed, C-H bend, C-C bend, C-O bend
-	858	883 w, 856 m	υ(C-O-C)
793	-	789 m	C-C bend
703	703	739 s, 707 s	COO-bend
408	409	406 m	O=C-O bend

Intensity abbreviations: sh: shoulder; w: weak, m: medium, s: strong, vs: very strong, vvs: very very strong.

This enabled us to recognize the spectral features of the drug in the ointment and in the skin. Figure 11 depicts the experimental Raman spectra of BA, the BA containing ointment, BA-free ointment, and the individual components of the ointment in the wavenumber range 1550-200 cm^{-1} to identify the spectral features of the API in the formulation. For example, the presence of two characteristic peaks of BA (739 and 707 cm^{-1}) confirms the BA content of the ointment.

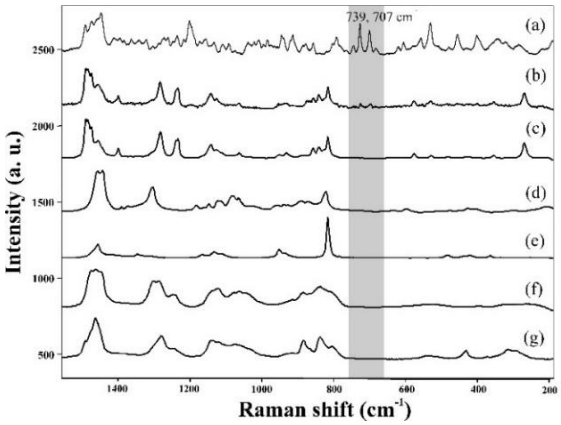

Fig. 11. Experimental Raman spectra of BA (a), BA containing ointment (b), BA-free ointment (c), isopropyl myristate (d), isopropyl alcohol (e), Labrasol (f) and Transcutol (g).

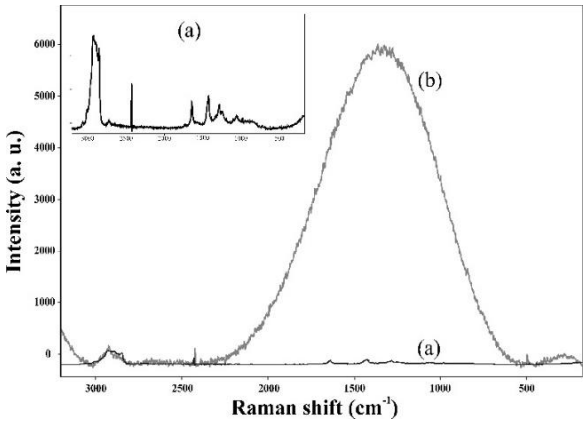

Fig. 12. Experimental Raman spectra of non-treated hairless mouse skin (a) and the fluorescent spectra of BA-treated skin (b).

However, for the measurements of BA and BA-containing formulations' spectra, we needed to use different parameters, because we observed remarkable fluorescence of the

drug. BA shows very weak intensity compared to the skin signal, but the observed fluorescent signal of the molecule using the above-mentioned excitation source can be the indicator of the drug. The untreated skin itself does not show fluorescence, so the appearance of this signal can be connected to the presence of the active agent (Figure 12).

5.2.2. Distribution maps of betulinic acid in the skin

Raman spectra were acquired from skin treated with BA ointment and from non-treated intact *ex vivo* skin as a control, both perpendicular to the SC at equivalent depth and width (700x30 μm).

Figure 13 displays qualitative distribution maps of BA in skin specimens after different EP protocols. Our aim was to determine whether the penetration depth of BA can be ameliorated by the use of different EP protocols. As the skin sections were planar, there was no need for the confocal z-axis and adjustment of the depth values. The whole skin thickness of a hairless mouse is about 0.7 mm [79,80], therefore 700 μm deep sections of the skin specimen were investigated, from top to bottom corresponding to the SC (5-9 μm [60]) → epidermis (about 29 μm [80]) → dermis.

In order to confirm BA penetration, the chemical maps were determined. The characteristic fluorescent signal was used to visualize the spatial distribution of BA from the Raman chemical mapping. The identification of the active agent was achieved by using a multivariate curve resolution with alternating least squares chemometric method. This method provides the response profiles of the examined component in complex samples and provides qualitative information about the spatial distribution.

The presence of the fluorescent signal due to BA in the skin indicates the distribution of BA following conventional treatment. This signal is weak and almost all of the upper layers of the skin are affected (Figure 13A). Without EP, the epidermal and upper dermal regions serve as a tight barrier limiting the diffusion of BA. Thus, a slow and lower amount of BA diffusion took place. After 1 min 900 V EP treatment, BA penetration was remarkably deeper and showed better distribution approximately in the whole skin section (Figure 13B). The BA content of the skin specimen (to a depth of 700 μm) was relatively lower after the 900 V 2 min EP treatment, mostly present in the upper layers of the epidermis and the deeper regions (Figure 13C)**.** After 6 min 900 V treatment, the drug disappeared from the upper layers and was present in the undermost layers of the dermis, indicating the penetration to deeper regions, and presumably potential to systematic absorption (Figure 13D).

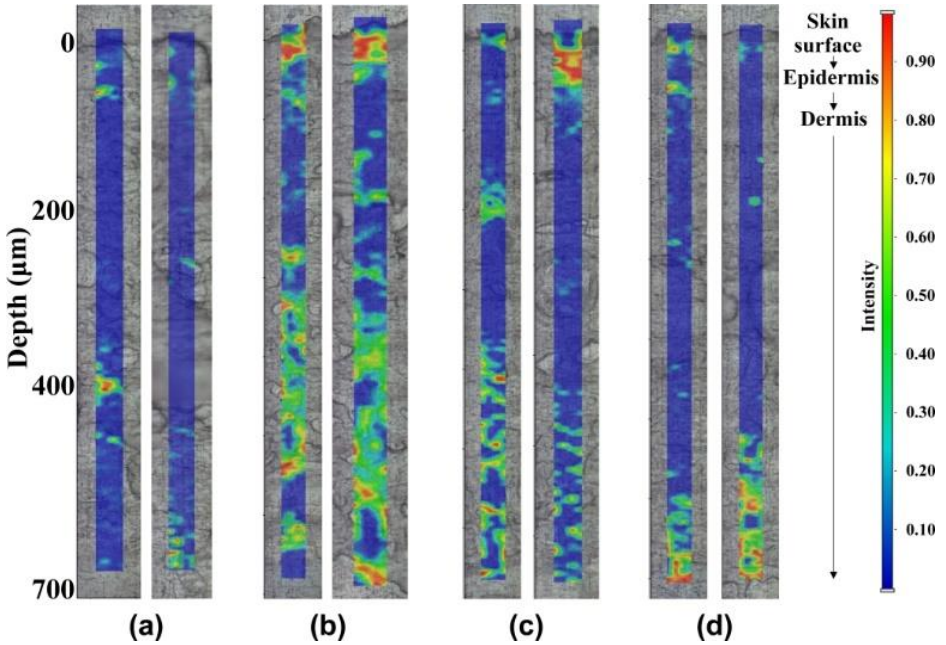

Fig. 13. Qualitative Raman maps of BA distribution in animal skin specimens following different EP protocols. Conventionally treated skin as control (a), skin treated with EP at 900 V for 1 min (b), for 2 min (c) and for 6 min (d). Color coding of BA-content: red>yellow>green>blue.

5.3. Investigation of the properties and performance of lidocaine-containing formulations

5.3.1. Characterization of the carrier systems

5.3.1.1. Liposome

5.3.1.1.1. Particle size and zeta potential measurements

The light scattering analysis showed that the size of liposomes were in the range of 1844± 562.9 nm to 4842± 275.57 nm. The results presented a decrease in vesicle size and a reduction in homogeneity with increasing amount of LID, as indicated by the growth of the polydispersity index (Table 3). The PDI of the investigated vesicles showed values from 0.279± 0.253 to 1.000± 0.000, representing heterogeneous populations (PDI> 0.3) of vesicles [40].

These findings could be explained by considering that the drug will be located within the liposomal bilayer and could alter the microstructure of the vesicular membrane, thus reduce the liposomal membrane organization.

Table 3. Particle size and zeta potential of LID-liposomes (p< 0.05*, p<0.01** and p < 0.001***).

LID content (wt %)	Mean particle size (nm) ± SD	Polydispersity index ± SD	Zeta potential (mV) ± SD
0	4842 ± 275.57	0.374 ± 0.085	-0.035 ± 0.814
1	3875 ± 231.2	0.279 ± 0.253	-1.768 ± 1.617
2	3211 ± 354.3*	0.348 ± 0.379	-0.875 ± 2.288
3	2671 ± 523.9**	1.000 ± 0.000	0.907 ± 2.007
4	2314 ± 998.9***	0.463 ± 0.366	-1.283 ± 1.064
10	1844 ± 562.9***	0.534 ± 0.483	-0.575 ± 0.827

On the other hand, measurements of zeta-potential values showed that it was barely influenced by the presence of the drug, so a contribution of the drug to the liposomal charge can be excluded (Table 3). Therefore, the nearly zero charge of the vesicles could be attributed to the properties of the DMPC molecules, which is a zwitterionic lipid that, at physiological pH, forms membranes with practically zero surface charge density [41]. The slight difference in the values could be explained by the measurement difficulties around the value zero.

5.3.1.1.2. DSC investigation

The effect of LID on the thermotropic behavior of DMPC was investigated by DSC as a function of the anesthetic concentration. Figure 14 shows the heating curves of the multilamellar DMPC vesicles in the absence and presence of different amounts of LID up to 10 wt%.

Table 4 gives the T_m (main transition temperature) and ΔH (enthalpy of transition) values measured in all the formulations, in the heating cycles.

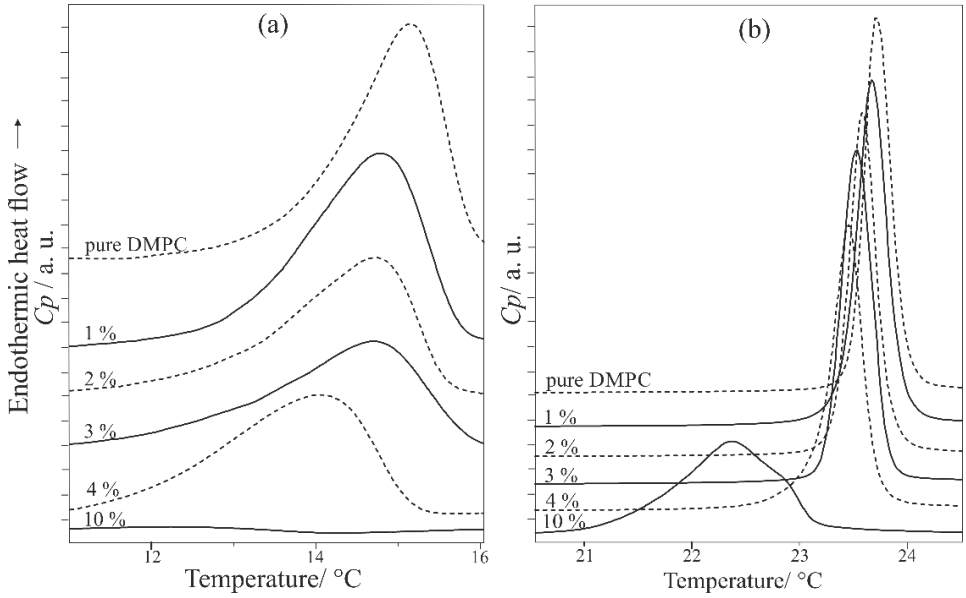

Fig. 14. DSC curves of the liposomes showing the pre-transitions (a) and main transitions (b).

Table 4. Main transition temperature and enthalpy values of the formulations.

Lipid (mg mL^{-1})	LID (wt%)	LID (mM)	$T_m \pm$ SD (°C)	ΔT_m (°C)	$\Delta H \pm SD$ (cal mol^{-1})
5	0%	0.000	23.85 ± 0.0012	0.00	5293 ± 26.3
5	1%	0.213	23.79 ± 0.0012	0.06	5535 ± 26.8
5	2%	0.427	23.72 ± 0.0011	0.13	4931 ± 23.4
5	3%	0.640	23.68 ± 0.0010	0.17	5386 ± 20.4
5	4%	0.853	23.62 ± 0.0024	0.23	4689 ± 44.1
5	10%	2.134	22.66 ± 0.0035	1.19	5297 ± 34.4

The T_m and ΔH values measured in pure DMPC liposomes (23.85 °C, 5293 cal mol^{-1}, respectively) were in good agreement with the literature data [81].

The pre-transition peak is broad, nearly symmetrical and, because of the formation of an intermediate meta-stable phase, slowly turns into the lamellar gel phase [83]. This peak became smaller by the addition of LID and disappeared at the concentration of 10 wt%. The vanishing nature of the pretransition is common upon the addition of membrane solutes [84,85].

The most outstanding feature of the series of curves is that the main phase transition for DMPC -represented by the peak of *Cp*- is progressively lowered and broadened with increasing concentrations of LID. The position of the main peak is reduced from *Tm*=23.85°C for pure DMPC to 22.66°C with 10 wt% LID. This suggests a chain disordering effect in the lipid membrane (Figure 15).

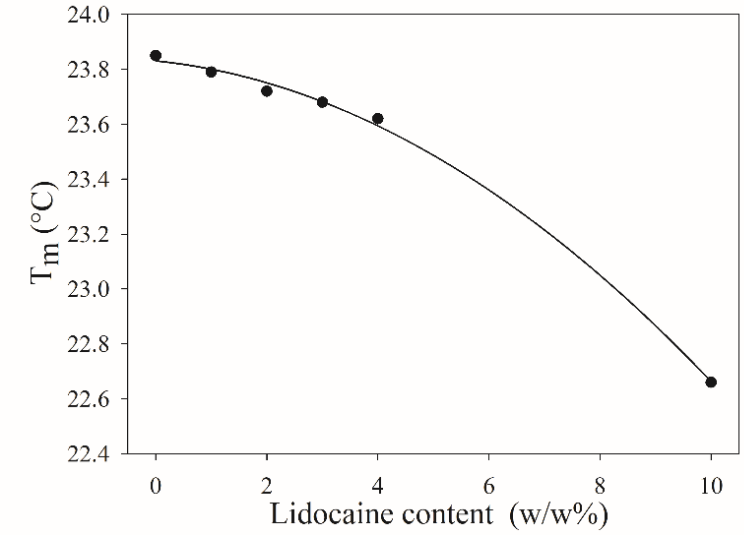

Fig. 15. Phase transition temperatures of DMPC bilayers as a function of LID concentration.

The analysis of ΔH, given by the peak area, can provide information about the impact (location) of the LID molecules in the phospholipid bilayers. In the investigated systems LID does not affect ΔH but causes a decrease in T_m. This can be explained by a superficial interaction between the LID and the DMPC molecules and/or the intercalation of LID molecules between the chains of the lipids without reducing the stability of the membrane [82].

5.3.1.1.3. Encapsulation efficiency

The encapsulation efficiency values of the liposomal formulations obtained by different experimental methods are represented by Figure 16 and Table 5.

The results are quite ambiguous. With the most widespread indirect method, we measured notably higher EE % values (9.4-32.2%) and the measurements also resulted

high standard deviation, while the results of the direct method (3.5-10.1%) and the DSC measurements (5.4-13.0%) correlate nicely. These differences could be explained by some possible experimental errors in connection with the indirect method. First of all, the indirect method is a derived result, and it is evident that each experimental step and each further calculation will introduce an experimental error, moreover, may cause a loss of product (for example adsorption on the vial wall or pipette tips). The other probable explanation is the imperfect separation and the presence of liposomes in the supernatant as well.

According to Nernst's partitioning law for dilute solutions, the ratio of concentrations in two separated phases is the constant partition coefficient (K_R). The calculated average K_R values are also similar for the direct and DSC methods (0.00903±0.00455 mM^{-1} and 0.00895±0.00468 mM^{-1}) and different for the indirect method (0.0375±0.0306mM^{-1}).

Table 5. Encapsulation efficiency ($p< 0.05$*, $p<0.01$** and $p < 0.001$*** vs. indirect method).

LID (wt %)	Indirect method		Direct method		DSC	
	EE%± SD	K_R (mM^{-1})	EE%± SD	K_R (mM^{-1})	EE%	K_R (mM^{-1})
1	29.0% ± 9.3	0.0553	10.1% ± 4.2*	0.0152	6.6%*	0.0095
2	32.2% ± 7.4	0.0645	5.6% ± 1.9***	0.0080	6.4%**	0.0092
3	32.0% ± 10.3	0.0637	4.4% ± 1.8**	0.0063	6.1%**	0.0087
4	22.4% ± 14.1	0.0392	3.9% ± 2.6	0.0055	5.4%	0.0077
10	9.4% ± 15.4	0.0140	3.5% ± 3.2	0.0049	13.0%	0.0203

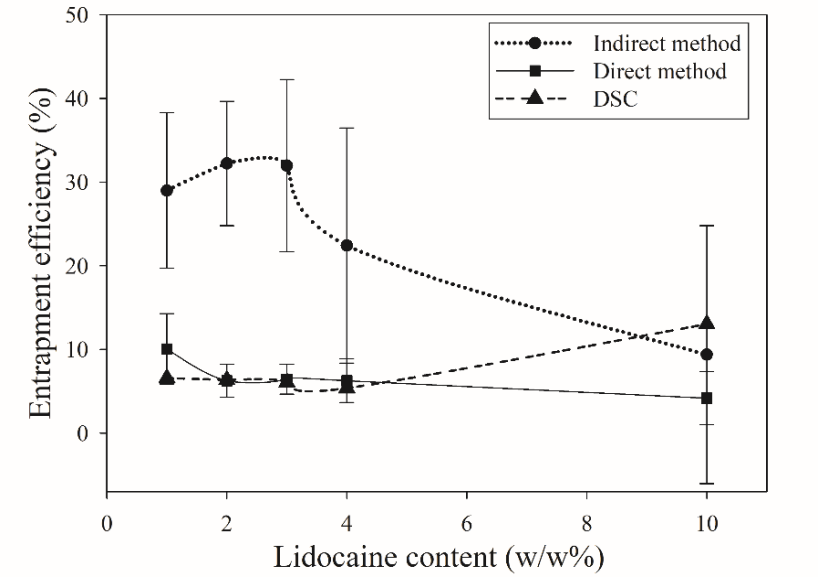

Fig. 16. Drug encapsulation efficiency obtained by different experimental methods.

Considering these outcomes, we can conclude that the direct method and DSC confirmed each other's results, while the indirect method suffered from an unknown error source.

5.3.1.2. Lyotropic liquid crystal

5.3.1.2.1. Polarization Microscopic Examinations

Figure 17 represents a polarized microscopic picture of the developed blank and LID-containing LLC structures, revealing a lamellar LLC pattern with a characteristic „Maltese cross" structure in polarized light [86]. Liquid crystals are anisotropic materials and they display characteristic textures between crossed polarizers under an optical microscope. These textures can be used to identify different liquid crystalline phases. Liquid crystals are visible by polarizing light microscopy as lipid circular droplets with characteristic birefringence in the shape of a Maltese cross. The presence of the Maltese cross indicates a parallel orientation of one of the main axes of the structure in the plane of polarization of the incident light, so linearly polarized light passing through will not change its polarization, resulting in dark regions [87].

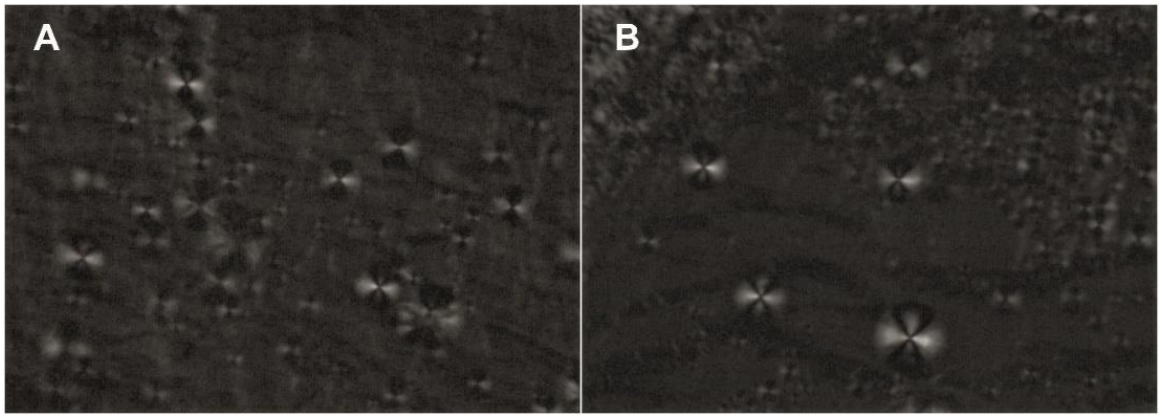

Fig. 17. Polarizing microscopic examination of blank (A) and lidocaine containing (B) LLC.

5.3.1.3. Nanostructured lipid carrier

5.3.1.3.1. Results of particle size and zeta potential analysis

The particle size of the LID-containing NLC system was 87.61±0.55 nm. The calculated polydispersity index was 0.1615±0.01, referring to a monodisperse distribution [88,89]. The low polydispersity index predicts a satisfying stability of the system [37]. The zeta potential was -11.983±0.31 mV.

5.3.1.3.2. Spectral signatures of lidocaine as free base or salt

The first part of the Raman study consisted of establishing spectral signatures for LID and for LID-containing formulations. Figure 18 presents the spectra of LID base and LID hydrochloride. This enabled us to determine the most pertinent spectral features to detect the drug in the cross-sectioned skin. The characteristic bands of different LID forms are presented in Table 6 with the vibrational assignments (cm^{-1}) based on Ref. [90].

Table 6. Observed Raman peaks (in cm^{-1}) and peak assignments for lidocaine base and hydrochloride.

Observed peaks[a]		
Raman LID base	LID hydrochloride	Assignment
3043 (m)	3042 (m)	methyl antisymmetric stretching
	2979 (vs)	methyl antisymmetric stretching
2922 (vs)	2924 (vs)	CH_2 antisymmetric and symmetric stretching
2875 (m)		methyl symmetric stretching
		CH_2 symmetric stretching
1664 (s)	1670 (s)	C=O stretching
	1656 (s)	HNC scissor deformation
1594 (s)	1593 (m)	HNC scissor deformation, NC amide stretching
		methyl antisymmetric deformation
1484 (m)	1471 (m)	methyl antisymmetric deformation
1452 (vs)	1449 (m)	CH_2 scissor deformation
		methyl symmetric deformation
		CH_2 wag
	1436 (m)	methyl symmetric deformation
1376 (m)		CH_2 twist, CH_2 wag
		ring stretching deformation III, CH_2 twist, CH_2 wag
		CH_2 twist
	1388 (s)	CH_2 wag
	1311 (m)	CH_2 wag, CH_2 twist
	1299 (w)	CH_2 twist
	1275 (m)	m-CH in plane bend
1264 (vs)	1262 (s)	m-CH bend, o-CC symmetric stretching
1215 (m)		amide NH stretching, CC stretching
1164 (m)	1163 (w)	NC_2 antisymmetric stretching, CH_2 rock, CH_2 twist
		m-CH bend, ring stretching deformation II
	1155 (w)	NC_2 antisymmetric stretching
1094 (s)	1095 (s)	methyl rock, CH_2 twist
	1047 (m)	methyl rock
991 (m)	992 (m)	CH_2 rock, CH wag
972 (w)		CH wag
958 (w)	953 (w)	CC stretching, NCO scissor deformation
909 (vw)	894 (vw)	CC stretching
880 (vw)	872 (vw)	ring bend deformation, ring N-stretching
	856 (w)	CH_3 rock
		CH wag
	780 (vs)	CH_2 rock
		NC_2 symmetric stretching
754 (w)		ring torsional deformation, HNC wag
705 (vs)	692 (vs)	HNC wag
661 (m)		ring stretching deformation,
616 (vvs)	608 (s)	NCO wag
513 (vw)	516 (vw)	ring torsional deformation II
	539 (m)	CCC in plane bending
	557 (m)	ring bending deformation III
		NCO twist
486 (w)		ring bend deformation II
	456 (s)	o-CC bend
		CH_2 rock
	410 (m)	NC_2 wag
		CCC in plane bending
232 (s)	241 (s)	o-CC wag

[a] Intensity abbreviations: vw: very weak, w: weak, m: medium, s: strong, vs: very strong, vvs: very very strong.

Both LID base and hydrochloride showed characteristic peaks around 2922, 1594, 1452, 1264, 1094 and 705 cm^{-1}. The intense peak at ~2922 cm^{-1} represents the methylene CH_2 stretching in the two ethyl groups. HNC scissoring and NC stretching modes are noted in the spectra as the peak at ~1594 cm^{-1}. The peak at ~1452 cm^{-1} represents methylene scissoring. One of the most intense bands in the spectra was observed at ~1263 cm^{-1}, arising from the CH bending and C–C symmetric stretching modes. Methyl rock, CH_2 twist and NC_2 symmetric stretch are present in the spectra as a strong peak at 1094 cm^{-1}. There is also a very strong peak at ~705 cm^{-1} in the Raman spectrum representing HNC wag and twist of ring torsional deformation. In case of LID-HCl, most of these characteristic vibrations slightly shifted because of the coordination of H^+ to the amino group.

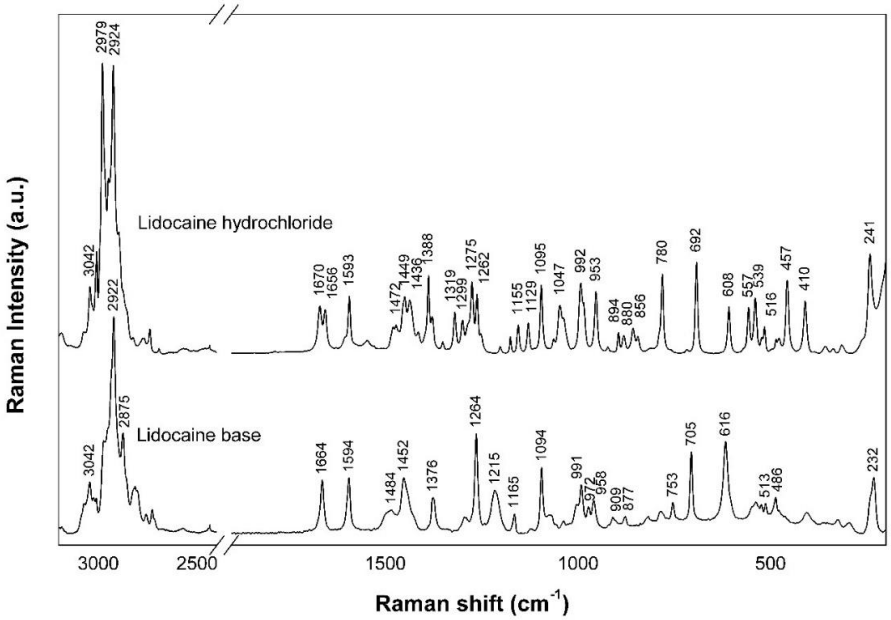

Fig. 18. Raman spectra of the lidocaine base and hydrochloride salt form with the indication of the peak positions.

5.3.1.3.3. Investigation of lidocaine-carrier system interactions

For the determination of LID-excipient interactions in the NLC formulation at the level of functional groups, we applied FT-IR and Raman spectroscopy. FT-IR and Raman spectra of each excipient, LID, LID-free NLC and LID-NLC formulations were studied as shown in Figure 19.

The 1497 cm^{-1} peak, related to the methyl functional groups of LID, is present in the FTIR spectra of LID-NLC, but absent from the spectra of the blank NLC, indicating the presence of LID in the lipid nanoparticle.

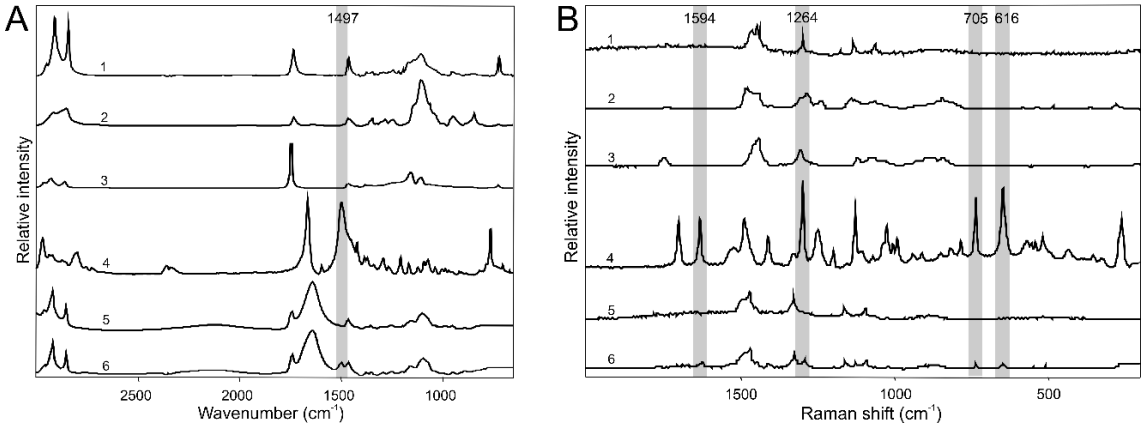

Fig. 19. FT-IR (A) and Raman (B) spectra of individual components and NLC compositions. Notes: Apifil (1), Cremophor RH60 (2), Mygliol 812 N (3), Lidocaine (4), Lidocaine-free NLC (5), Lidocaine NLC (6).

All the characteristic peaks of the drug and the excipients were present in the LID-NLC spectrum and no shifting of existing peaks or creation of new peaks were observable. This indicates that there were only physical interactions between the drug and the excipients, and no chemical interaction took place among them. The Raman measurements confirmed these results: the peaks at 616, 705, 1264, 1594 cm^{-1}, which are the characteristic features of the LID spectra, are present in the LID-NLC spectra without shifting, and they are missing from the blank NLC. The absence of chemical interactions between the drug and the vehicle suggests that the release of LID from the carrier system is not inhibited.

5.3.2. Comparative study of lidocaine-containing formulations based on QbD approach

5.3.2.1. Definition of QTPP and CQAs for a dermal local anesthetic formulation

We aimed to select the best semisolid local anesthetic formulation for dermal use, which can provide effective and prolonged anesthesia. This therapeutic efficacy of the formulations depends on therapeutic indication, route of administration, site of activity, dosage form, release profile, stability and dosage strength. The quality attributes were identified as physical attributes, the solubility of API in the drug product, homogeneity of API in the drug product, *in vitro* drug release, *ex vivo* drug release, moisturizing effect, TEWL, dosage form type and viscosity. Table 7 presents the list of QTPP and CQA parameters with their targets and justifications. The Ishikawa diagram was constructed to identify the effect of key material attributes and process parameters for the optimized development of semisolid systems (Figure 20).

Table 7. QTPP and CQAs of the target local anesthetic formulation.

QTTP parameters	Target	Justification
Therapeutic indication	local anesthetic	Local anesthesia and pain alleviating are required in various minor surface-skin surgical conditions and invasive procedures. Local anesthetics are also available to provide temporary relief from pain, irritation and itching caused by various conditions.
Route of administration	Dermal	The dermal delivery of drugs is an opportunity to avoid systemic side effects and the hepatic metabolism of drugs, thus the application of lower doses is available. Furthermore, it is a non-invasive, easy-to-use method resulting in high patient compliance.
Site of activity	Topical	The topical activity of local anesthetic drugs is desired because of their systematic side effects. Topical formulations are designed to allow the dermal penetration of their actives into the deeper regions of the skin, such as the viable epidermis and the dermis, where the nerve fibers are located. The absorption into the systemic circulation is not the aim of these formulations.
Dosage form	Semisolid system	Semisolid systems offer many advantages, like easy application and pleasing rheological behavior, which enable them to adhere to the application surface and they are able to topically deliver many drug molecules.
Release profile	Sustained drug release	Prolonged duration local anesthesia is desirable to effectively treat pain and to reduce the number of applications, thus improving patient compliance.
Stability (physical, chemical, biological)	no visible sign of instability at the time of preparation and after 1 months (at room temperature)	It is essential to maintain the physical, chemical and biological stability of the product over time because stability issues, like phase separation, change in pH, viscosity, appearance and crystal formation can affect the release and therapeutic effect of the formulation.
Dosage strength	5g/100g	5% lidocaine formulations are effective as local, topical anesthetic preparations.
CQA	**Target**	**Justification**
Physical attributes (color, odor, appearance)	Clear, translucent or opaque appearance, and odorless smell	Physical attributes are not critical, but satisfactory appearance can improve patient compliance. However, they are not directly in connection with safety and efficiency.
Solubility of API in drug product	High (>90 %)	Drug solubility provides uniformity of dosage form by preventing phase separation. Furthermore, a high concentration gradient can increase the diffusion force across the skin.
Homogeneity of API in drug product	Homogenous distribution of the API	Homogeneity is crucial to provide the uniformity of dosage units during the application period.
In vitro drug release	Sustained (compared to control)	Slow drug release is required to provide prolonged anesthesia.
Ex vivo drug release	Sustained (compared to control)	Slow drug release is required to provide prolonged anesthesia. Permeability is less through human skin than synthetic membrane based on preliminary results in the literature.
Moisturizing effect	Increase of basal skin hydration (compared to control)	An increase of the water content of the skin promotes drug permeation.
TEWL	Minor and transient change in TEWL values (compared to control)	A high value of transepidermal water loss is related to the disruption of the barrier function of the skin.
Viscosity	Optimal spreadability of the product (range: 1000-50000 mPas)	Rheological properties, such as the viscosity of semisolid dosage forms, can influence their drug delivery. Viscosity may directly influence the diffusion rate of drug at the microstructural level.
Dosage form type	Penetration enhancing properties	The composition and the special structure of the vehicle can ameliorate the penetration of active agents.

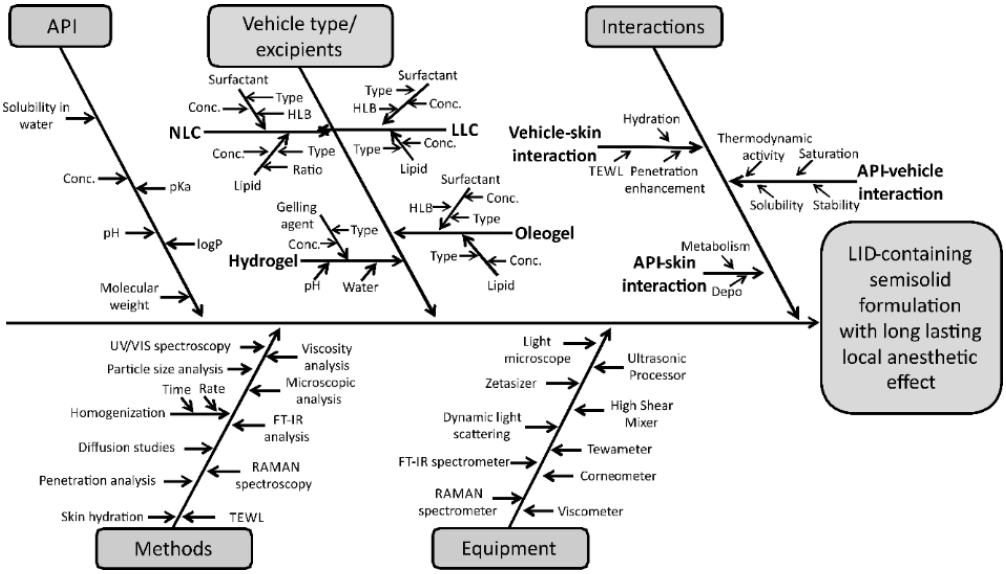

Fig. 20. Ishikawa diagram.

5.3.2.2. Initial risk assessment

Initial RA identified the CQAs of product quality expectation. The risk estimation matrix presents the interdependence rating between the QAs and QTPPs on the three-level scale (Table 8). For the probability rating, a 1 (low)-3 (medium)-9 (high) scale was used, considering all CQAs and their relationship to the QTTPs. The following properties were found to influence product quality: *in vitro* and *ex vivo* drug release (both 18 %), dosage form type (15 %), moisturizing effect and TEWL (both 13 %). Based on the REM results, a Pareto chart (Figure 21) was generated showing the severity scores of CQAs, which lead us to the following findings: *in vitro* and *ex vivo* drug release, dosage form type, moisturizing effect and TEWL with the highest severity score (>300) are the most critical characteristics influencing the quality of the formulation. The Pareto chart illustrates the critical attributes which have to be considered during the development process. Based on the results of the RA, these points have been investigated in this research.

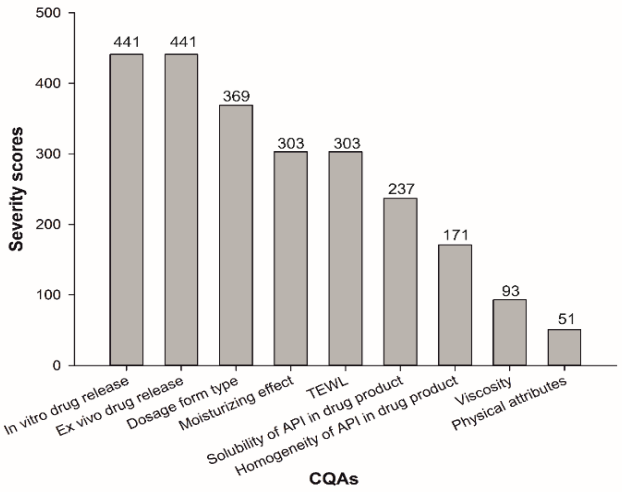

Fig. 21. Pareto analysis of the identified CQAs.

Table 8. Selected QTPPs and CMAs representing their interdependence rating with risk estimation matrix (Lean-QbD Software): Low = low-risk parameter; Medium = medium-risk parameter; High= high-risk parameter.

CQA \ QTPP		Dosage form (H)	Route of administra-tion (H)	Site of activity (H)	Therapeutic indication (H)	Release profile (H)	Stability (M)	Dosage strength (M)
Physical attributes	2%	Low	Low	Low	Low	Low	Low	Low
Solubility of API	10%	High	Low	Low	Medium	High	Low	High
Homogeneity of API in drug product	7%	Medium	Low	Low	Medium	High	Medium	Medium
In vitro drug release	18%	High	High	High	High	High	Medium	High
Ex vivo drug release	18%	High	High	High	High	High	Medium	High
Moisturizing effect	13%	High	High	Medium	High	Medium	Low	Low
TEWL	13%	High	High	Medium	High	Medium	Low	Low
Viscosity	4%	Medium	Low	Low	Low	Medium	Medium	Low
Dosage form type	15%	High	High	Medium	High	High	Medium	Medium

5.3.2.3. Results of *in vitro* release and *ex vivo* permeation studies

In Figure 22, the plots of the cumulative amount of LID permeated through artificial mixed cellulose ester membrane (A) and human HSE (B) as a function of time are shown. Steady-state flux values of formulations are reported in Table 9.

The *in vitro* diffusion of LID through the artificial membrane from the different formulations is illustrated in Figure 22A. The LLC formulation showed a complete release of LID at the end of 15-18 h. The conventional hydrogel exhibited a fast onset of diffusion, but it was not completed after 24 h (78.58±2.50%). The oleogel and NLC formulations provided a sustained release, 70.32±1.76% of the drug was released from the oleogel, 58.66±4.28% from NLC after 24 h.

Ex vivo penetration patterns were slightly different, presumably because of the interaction of the different vehicles and the skin lipids and proteins (Figure 22B). LID permeation from the oleogel exhibited the lowest value, only 9.84±1.37% of the drug penetrated after 24 h. There was no significant difference between the penetration of conventional hydrogel (15.05±3.70%) and LLC (14.12±1.73%) formulations. Surprisingly, through the epidermis, the NLC exhibited the most complete penetration (19.44±5.05%), whereas *in vitro* it was the lowest. This finding could be explained by the special structure of the NLC, which allows the high bioavailability of this formulation [91]. The components of the NLC formulation have similar lipophilicity as the skin, so they have good miscibility with the skin lipids, and this can cause greater permeation [92].

Our results are in good agreement with other studies, which revealed that lipid nanocarriers can improve penetration and effectiveness of encapsulated LID [91,93–95]. The high permeation rate of LID through the epidermis predicts the fast accumulation of the drug in the dermis, which is the site of action for local anesthetics. Babaei et al. confirmed that NLC can penetrate through the epidermis and accumulate in the dermal layers of the skin [96]. The low permeation rates of oleogel could be explained by their composition: they do not contain any water (in contrast to the other formulations), so there will be no external supply of water, hydration can only be provided from the internal processes of the skin [97].

Table 9. Steady-state flux of LID *in vitro* and *ex vivo* from different carrier systems.

	Flux (μg cm^{-2} h^{-1})	
	in vitro	*ex vivo*
Conventional hydrogel	2175.59	369.23
Oleogel	1844.57	259.66
LLC	3211.42	373.99
NLC	1682.02	618.05

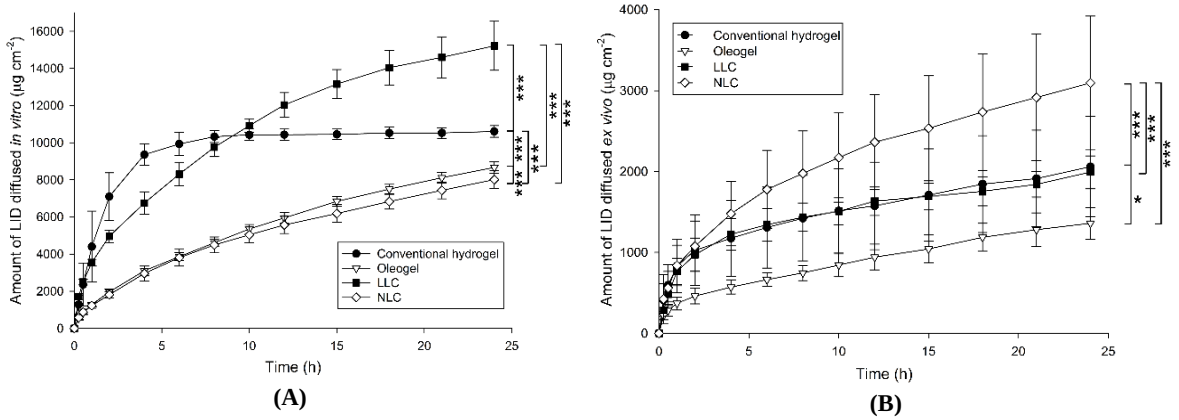

(A) **(B)**

Fig. 22. *In vitro* (A) and *ex vivo* (B) diffusion studies of LID containing formulations ($p< 0.05$*, $p<0.01$** and $p < 0.001$***).

5.3.2.4. Skin hydration and TEWL measurements *in vivo*

In skin hydration measurements (Figure 23A), there were no significant differences between the hydrating effect of conventional hydrogel and LLC. Both of them increased the hydration slightly after 30 min (13.63±5.23% and 18.42±3.12%), but this effect was shortened after 150 min (6.92±5.88% and 11.78±3.95%). However, oleogel caused a dramatic decrease of hydration after 30 min (-43.47±5.93%). This could be the result of the presence of Kolliphor RH40 in the formulation, which is a well-known penetration enhancer that disturbs the ordered lipid structure of the SC, resulting in the loss of water content [27]. Furthermore, in the oleogel formulation, there was no water as an excipient, so after the application, there is no chance to supply the lost water from this source. After

150 min, the skin barrier seemed to have recovered partially, and the hydration value (-27.57±6.03 %) was closer to the initial level. NLC resulted in a remarkable increase in skin hydration after 30 min (71.18±3.31%) and the hydration maintained a high level also after 150 min (64.65±5.46 %).

The TEWL changes displayed notable differences between the formulations (Figure 23B). NLC caused the slightest increase in TEWL (14.68±3.19% after 30 min, 18.46±2.45% after 90 min and 22.78±7.39% after 150 min). It is well-known that lipid nanocarriers with a particle size less than 200 nm form a lipid film on the skin surface, and owing to this occlusive effect, the TEWL changes will decrease, thus hydration will increase [98]. Our results confirmed these findings and are in good agreement with the *ex vivo* penetrations studies because improved skin hydration and occlusion are shown to increase drug absorption from topical formulations [99].

Conventional hydrogel caused a slightly noticeable TEWL increase after 30 min (36.20±11.25%), but this effect was reduced after 150 min (19.71±5.71%). However, oleogel increased TEWL significantly (51.24±6.66% after 30 min,67.33±9.06% after 90 min and 67.73±3.54% after 150 min), which can explain the dramatic decrease in hydration values discussed earlier. The TEWL rise was the most significant for LLC. The increase was 101.39±4.24% after 30 min, and it still rose after 150 min to 130.08±7.95%. The reason for this huge water loss is definitely the high amount of surfactant (Kolliphor RH40) incorporated in the LLC formulation. However, skin hydration was not negatively affected because of the lamellar, water-containing structure of the LLC, which can provide excellent hydration and compensate the high TEWL values [100].

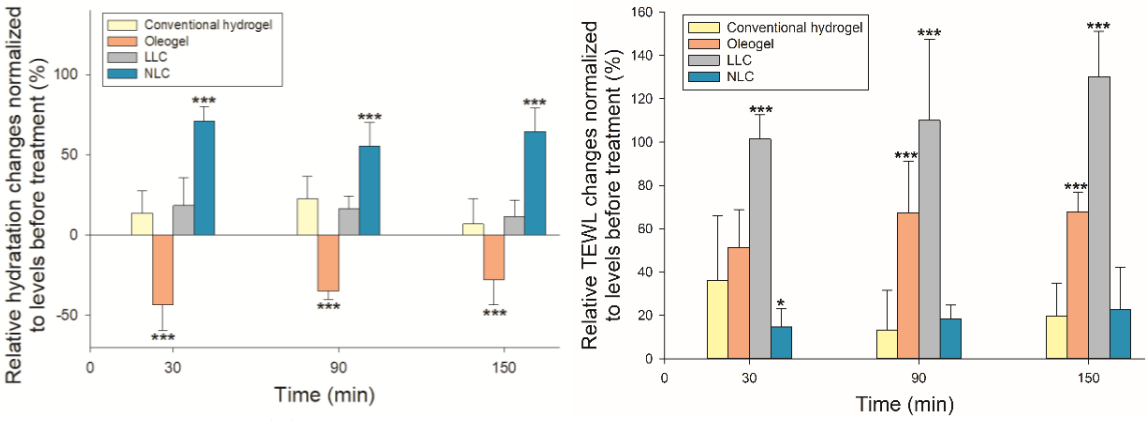

(A) **(B)**

Fig. 23. Skin hydration (A) and TEWL (B) changes after exposure to formulations. Values are given as percentage referring to values before treatments. ($p< 0.05$*, $p<0.01$** and $p < 0.001$*** vs. conventional hydrogel)

5.3.3. Following-up skin penetration of lidocaine-containing formulations *ex vivo*

5.3.3.1. Raman spectra of formulations

Figure 24 depicts the Raman spectra of the LID-free "blank" formulations and the LID-containing formulations in the wavenumber range of 1700-300 cm^{-1}. Highlights show the characteristic spectral features of LID which are present in the spectra of API containing formulations and absent from the blank one - they are the indicators of the presence of LID.

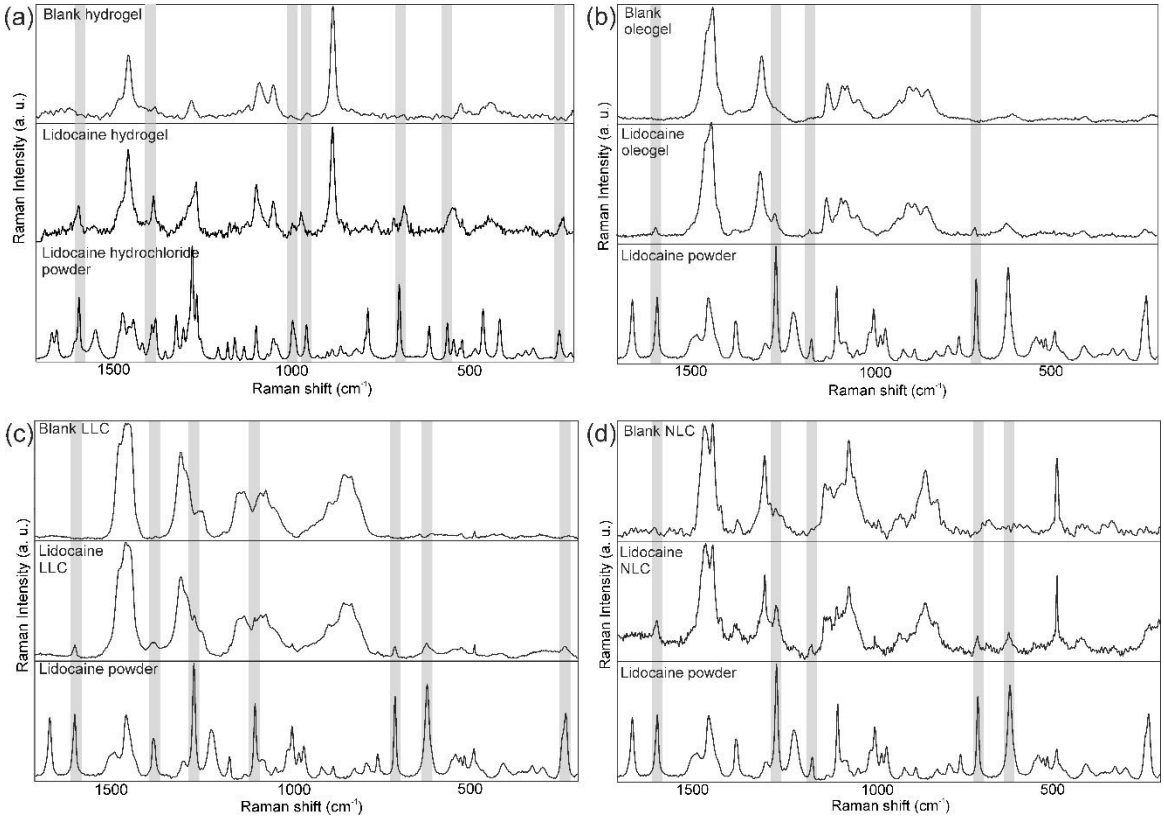

Fig. 24. Raman spectra of hydrogel (a), oleogel (b), LLC (c) and NLC (d) formulations.

5.3.3.2. Qualitative Raman maps of lidocaine distribution in *ex vivo* skin specimens

Figure 25 displays qualitative distribution maps of LID in human skin specimens after the treatment with hydrogel, oleogel, LLC and NLC formulation. Our aim was to determine whether LID diffusion is limited to the SC or it can penetrate into the epidermis or dermis. The full abdominal skin thickness of a healthy woman is around 2.28 mm [101]. From that, the SC is 6.3 μm and the total epidermis is 61.3 μm thick [102]. The thickness of dermal layers is around 1.84 mm [103].

The Raman spectrum of the skin is very complex and consist of many bands originating from different skin components, e.g. lipids, proteins and nucleic acids [104]. Many of these bands are overlapping with the peaks of the investigated formulations.

In order to confirm the presence of LID in the different skin layers, the spectral maps were resolved. The fingerprint region of the LID-containing formulations' spectra was compared with the spectra of treated and untreated skin spectra, and similarity was expressed as intensity. We created the distribution profiles representing the correlation between the map spectra (treated skin specimen) and the specified reference spectrum (fingerprint region of LID formulation spectra). The resulting correlation intensity values of the map spectra are analogous to the match values to the reference spectra. A higher intensity value indicates a greater similarity to the reference spectrum. A value of 1.0 indicates that the map spectrum and reference spectrum are identical.

The spatial distribution of LID is quite homogenous in the case of hydrogel and oleogel, the drug is present also in the epidermal and the dermal skin layers. In the case of oleogel, a slightly higher intensity is obtained, presumably because of the lipophilic nature of the carrier system, which predicts better penetration. It was proved by a study that oleogels were able to deliver a higher amount of diflunisal through the human skin than hydrogel [105]. The concentration profiles for oleogel showed a raised amount of LID in dermal layers and a continuous but slight increase from the outside to deeper skin zones is observable. However, low maximum intensity values predict a low amount of LID diffused even after 6 h.

LLC and NLC showed much higher intensity values in the treated skin specimens. The LID concentration at deeper skin layers was substantially increased compared to the surface. In the case of LLC, the drug is mostly localized in the dermal layers of the skin, presenting high intensity values. These results confirm the good penetration enhancer skills of LLC, due to their skin-similar structure and relatively high surfactant content, which is able to interrupt the skin barrier [40,106]. LLC contains a relatively high amount of Kolliphor RH40, which is a penetration enhancer surfactant that has a disordering effect on SC lamellar structure and disturbs the ordered lipid structure [27,107–110]. The dermal accumulation of LLC can ensure the sustained release of the API. It was proved before that LLC carrier significantly increased skin retention, delivered much higher amounts of drugs into the skin, thus demonstrating that the cutaneous absorption of drugs can be improved significantly by the LLC carrier [111]. Another lamellar LLC also showed relatively uniform distribution in the epidermis and the dermis with a small amount

present in the SC lamellar phase, the formulations showed much stronger signal in the dermal layer compared to the solution formulation [112].

In case of NLC, the drug is distributed in the whole skin section: it is present also in the epidermal and dermal layers and shows high intensity values. Because of the small particle size and lipophilic nature of NLC, it is able to penetrate through the skin more effectively, and presumably it interacts with skin lipids. Furthermore, because of the small particle size, lipid vesicles build a continuous film on the skin surface, which enhances penetration by an occlusive effect [36]. The good penetration of NLC systems to the epidermal and dermal layers was also confirmed by other studies [96,113].

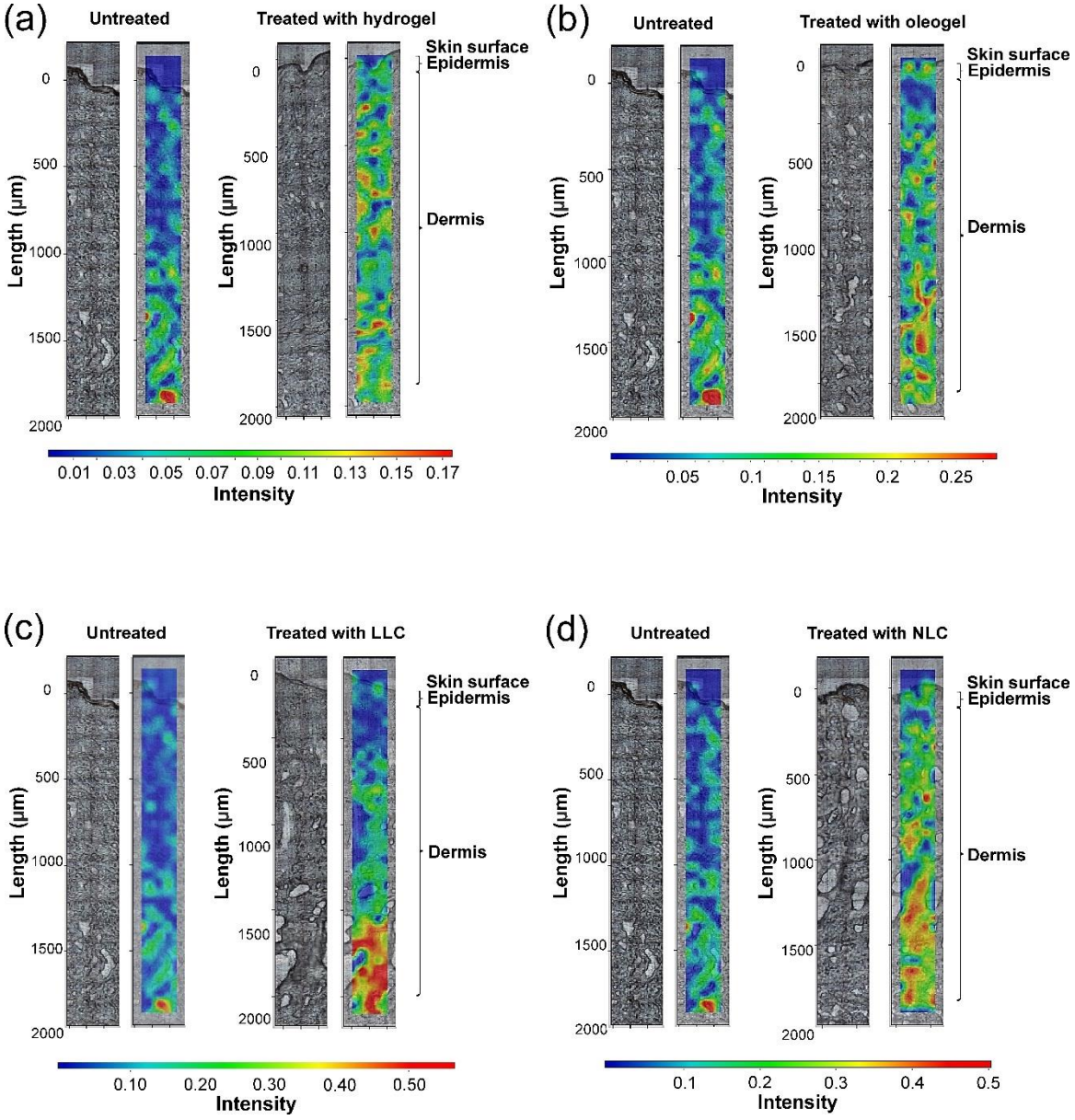

Fig 25. Video images and qualitative Raman maps of LID distribution in human skin specimens after 6 hours following treatment with hydrogel (a), oleogel (b), LLC (c) and NLC (d). Untreated skin is also displayed as a control in all cases. Color coding of content: red>yellow>green>blue.

6. SUMMARY

The aim of my Ph.D. work was to achieve a better understanding of active and passive skin penetration enhancement methods through investigating their effect on the penetration of novel anti-melanoma and local anesthetic formulations.

1. In the first part of my work, the applicability of stratum corneum lipid liposomes was investigated as possible *in vitro* model for investigating the effects of chemical penetration enhancers, such as Kolliphor RH40 and Transcutol.

   To summarize this part of my Ph.D. work, new results were achieved:

   - the concentration dependence of penetration enhancement by Kolliphor RH40 and Transcutol was demonstrated;
   - the mechanism of the disruption of the lamellar structure of skin modeling liposomes was revealed;
   - *in vitro-ex vivo* correlation was determined, thus the applicability of SCLLs as *in vitro* skin models was proved.

2. In the second part of my Ph.D. work, a possible non-invasive melanoma treatment was investigated. The effect of EP on the penetration of a plant-derived antitumor drug, betulinic acid (BA) incorporated in an ointment formulation was determined. The results led to the following conclusions:

   - the penetration depth of betulinic acid can be remarkably ameliorated by the use of electroporation;
   - the influence of various EP treatment times was proved, since they caused different spatial distributions of the drug in the skin;
   - after a 6-min EP treatment, a significant amount of BA reached the undermost layers of the dermis;
   - the combination of EP and BA can be a promising opportunity to treat tumors in the deeper skin regions in a non-invasive way.

3. In the third part of my thesis, different lidocaine-containing carrier systems were formulated and their properties and effects were compared using *in vitro, ex vivo* and *in vivo* methods. The use of the QbD concept during the development process revealed the critical points that should be investigated. The novelty of this work can be summarized in the following:

   - Quality Target Product Profile and Critical Quality Attributes were identified for the development of a dermal local anesthetic formulation, furthermore, an initial

risk assessment was done according to the Quality by Design methodology. The critical quality attributes influencing the quality and efficacy of the final drug formulation were then defined in order to select the control points;

- 3 types of novel nanostructured lidocaine carriers were successfully developed and characterized: liposomes, NLCs and LLCs;
- the encapsulation efficiency of lidocaine-containing liposomes was investigated using DSC. The results were compared with those obtained with ultracentrifugation. DSC method is more convenient compared to the techniques used generally for the determination of encapsulation efficiency in cases when phase transition measurements are made with the aim to obtain further information. This research revealed a less known application field of DSC, as a fast and reliable tool to determine EE%;
- among the investigated carrier systems, the nanostructured lipid carrier has proven to be the most promising vehicle for the topical delivery of lidocaine. It showed the best penetration properties through heat separated epidermis and the highest moisturizing effect, which are the most critical parameters based on the Quality by Design initial risk assessment and evaluation;
- the application of Raman spectroscopy provided the visualization of spatial distribution in the skin for different lidocaine-containing formulations. The results confirmed the raison d'ętre of developing modern carrier systems, as the nanostructured LLC and NLC showed noticeably better skin penetration compared with conventional hydrogel and oleogel;
- this work also highlighted the ability of Raman spectroscopy as a nondestructive technique for investigating skin distribution and tracking penetration pathways of active agents.

7. REFERENCES

[1] K.S. Siu, D. Chen, X. Zheng, X. Zhang, N. Johnston, Y. Liu, K. Yuan, J. Koropatnick, E.R. Gillies, W.P. Min, Non-covalently functionalized single-walled carbon nanotube for topical siRNA delivery into melanoma, Biomaterials. 35 (2014) 3435–3442. doi:10.1016/j.biomaterials.2013.12.079.

[2] R.L. Bronaugh, H.I. Maibach, W. Schalla, J.-C. Jamoulle, H. Schaefer, Percutaneous Absorption-Mechanisms-Methology-Drug Delivery, in: Percutaneous Absorpt., 2005: p. 878.

[3] R.H. Guy, Current status and future prospects of transdermal drug delivery, Pharm. Res. 13 (1996) 1765–1769. doi:10.1023/A:1016060403438.

[4] M.C.F. Simões, J.J.S. Sousa, A.A.C.C. Pais, Skin cancer and new treatment perspectives: A review, Cancer Lett. 357 (2015) 8–42. doi:10.1016/j.canlet.2014.11.001.

[5] C. Puglia, M.G. Sarpietro, F. Bonina, F. Castelli, M. Zammataro, S. Chiechio, Development, characterization, and in vitro and in vivo evaluation of benzocaine- and lidocaine-loaded nanostructrured lipid carriers, J. Pharm. Sci. 100 (2011) 1892–1899. doi:10.1002/jps.22416.

[6] K.S. Paudel, M. Milewski, C.L. Swadley, N.K. Brogden, P. Ghosh, A.L. Stinchcomb, Challenges and opportunities in dermal/transdermal delivery., Ther. Deliv. 1 (2010) 109–131. doi:10.4155/tde.10.16.

[7] A. Naik, Y.N. Kalia, R.H. Guy, Transdermal drug delivery: Overcoming the skin's barrier function, Pharm. Sci. Technol. Today. 3 (2000) 318–326. doi:10.1016/S1461-5347(00)00295-9.

[8] A. Alexander, S. Dwivedi, Ajazuddin, T.K. Giri, S. Saraf, S. Saraf, D.K. Tripathi, Approaches for breaking the barriers of drug permeation through transdermal drug delivery, J. Control. Release. 164 (2012) 26–40. doi:10.1016/j.jconrel.2012.09.017.

[9] J.A. Bouwstra, P.L. Honeywell-Nguyen, G.S. Gooris, M. Ponec, Structure of the skin barrier and its modulation by vesicular formulations, Prog. Lipid Res. 42 (2003) 1–36. doi:10.1016/S0163-7827(02)00028-0.

[10] E. Proksch, J.M. Brandner, J.M. Jensen, The skin: An indispensable barrier, Exp. Dermatol. 17 (2008) 1063–1072. doi:10.1111/j.1600-0625.2008.00786.x.

[11] J.A. Bouwstra, M. Ponec, The skin barrier in healthy and diseased state, Biochim. Biophys. Acta - Biomembr. 1758 (2006) 2080–2095. doi:10.1016/j.bbamem.2006.06.021.

[12] P.W. Wertz, Lipids and barrier function of the skin, Acta Dermato-Venereologica, Suppl. (1999) 7–11. doi:10.1080/000155500750042790.

[13] S.F. Taveira, R.F. V. Lopez, Topical Administration of Anticancer Drugs for Skin Cancer Treatment., in: Ski. Cancers - Risk Factors, Prev. Ther., 2011: p. 248–272.

[14] T. Haque, K.M. Rahman, D.E. Thurston, J. Hadgraft, M.E. Lane, Topical therapies for skin cancer and actinic keratosis, Eur. J. Pharm. Sci. 77 (2015) 279–289. doi:10.1016/j.ejps.2015.06.013.

[15] S. Labala, A. Jose, S.R. Chawla, M.S. Khan, S. Bhatnagar, O.P. Kulkarni, V.V.K. Venuganti, Effective melanoma cancer suppression by iontophoretic co-delivery of STAT3 siRNA and imatinib using gold nanoparticles, Int. J. Pharm. 525 (2017) 407–417. doi:10.1016/j.ijpharm.2017.03.087.

[16] S. Tadicherla, B. Berman, Percutaneous dermal drug delivery for local pain control, Ther. Clin. Risk Manag. 2 (2006) 99–113.

[17] L.N. Ribeiro, M. Franz-Montan, M.C. Breitkreitz, A.C. Alcantara, S.R. Castro, V.A. Guilherme, R.M. Barbosa, E. de Paula, Nanostructured lipid carriers as robust systems for topical lidocaine-prilocaine release in dentistry, Eur J Pharm Sci. 93 (2016) 192–202. doi:10.1016/j.ejps.2016.08.030.

[18] A.F. Rogobete, M. Dragomirescu, O.H. Bedreag, D. Sandesc, C.A. Cradigati, M. Sarandan, M. Papurica, S.E. Popovici, C. Vernic, G. Preda, New aspects of controlled release systems for local anaesthetics: A review, Trends Anaesth. Crit. Care. (2016) 4–11. doi:10.1016/j.tacc.2016.06.004.

[19] A.J. Claxton, J. Cramer, C. Pierce, A systematic review of the associations between dose regimens and medication compliance, Clin. Ther. 23 (2001) 1296–1310. doi:Doi 10.1016/S0149-2918(01)80109-0.

[20] P. Sakdiset, Y. Kitao, H. Todo, K. Sugibayashi, High-Throughput Screening of Potential Skin Penetration-Enhancers Using Stratum Corneum Lipid Liposomes: Preliminary Evaluation for Different Concentrations of Ethanol, J. Pharm. 2017 (2017) 1–10. doi:10.1155/2017/7409420.
[21] R.M. Hatfield, L.W.M. Fung, A new model system for lipid interactions in stratum corneum vesicles: Effects of lipid composition, calcium, and pH, Biochemistry. 38 (1999) 784–791. doi:10.1021/bi981421k.
[22] G.M.M.E. Maghraby, M. Campbell, B.C. Finnin, Mechanisms of action of novel skin penetration enhancers: Phospholipid versus skin lipid liposomes, Int. J. Pharm. 305 (2005) 90–104. doi:10.1016/j.ijpharm.2005.08.016.
[23] V.R. Sinha, M. Pal Kaur, Permeation enhancers for transdermal drug delivery, Drug Dev. Ind. Pharm. 26 (2000) 1131–1140. doi:10.1081/DDC-100100984.
[24] P. Sakdiset, H. Todo, K. Sugibayashi, Potential of stratum corneum lipid liposomes for screening of chemical skin penetration enhancers, Chem. Pharm. Bull. 65 (2017).
[25] J.E. Harrison, A.C. Watkinson, D.M. Green, J. Hadgraft, K. Brain, The relative effect of azone® and transcutol® on permeant diffusivity and solubility in human stratum corneum, Pharm. Res. 13 (1996) 542–546. doi:10.1023/A:1016037803128.
[26] A. Pandey, Role of Surfactants as Penetration Enhancer in Transdermal Drug Delivery System, J. Mol. Pharm. Org. Process Res. 2 (2014). doi:10.4172/2329-9053.1000113.
[27] S.H. Moghadam, E. Saliaj, S.D. Wettig, C. Dong, M. V. Ivanova, J.T. Huzil, M. Foldvari, Effect of chemical permeation enhancers on stratum corneum barrier lipid organizational structure and interferon alpha permeability, Mol. Pharm. 10 (2013) 2248–2260. doi:10.1021/mp300441c.
[28] A.C. Williams, B.W. Barry, Penetration enhancers, Adv. Drug Deliv. Rev. 56 (2004) 603–618. doi:10.1016/j.addr.2003.10.025.
[29] K. Bhise, S.K. Kashaw, S. Sau, A.K. Iyer, Nanostructured lipid carriers employing polyphenols as promising anticancer agents: Quality by design (QbD) approach, Int. J. Pharm. 526 (2017) 506–515. doi:10.1016/j.ijpharm.2017.04.078.
[30] C. Dianzani, G.P. Zara, G. Maina, P. Pettazzoni, S. Pizzimenti, F. Rossi, C.L. Gigliotti, E.S. Ciamporcero, M. Daga, G. Barrera, Drug delivery nanoparticles in skin cancers, Biomed Res. Int. 2014 (2014). doi:10.1155/2014/895986.
[31] B. Baroli, Penetration of nanoparticles and nanomaterials in the skin: Fiction or reality?, J. Pharm. Sci. 99 (2010) 21–50. doi:10.1002/jps.21817.
[32] G.J. Grant, M. Bansinath, Liposomal delivery systems for local anesthetics, Reg. Anesth. Pain Med. 26 (2001) 61–63. doi:10.1053/rapm.2001.19166.
[33] D.P.E. Cereda CM, de Araujo DR, Brunetto GB, Liposomal prilocaine: preparation, characterization, and in vivo evaluation, J Pharm Pharm Sci. 7 (2004) 235–40.
[34] P. Mura, F. Maestrelli, M.L. González-Rodríguez, I. Michelacci, C. Ghelardini, A.M. Rabasco, Development, characterization and in vivo evaluation of benzocaine-loaded liposomes., Eur. J. Pharm. Biopharm. Off. J. Arbeitsgemeinschaft Für Pharm. Verfahrenstechnik e.V. 67 (2007) 86–95. doi:10.1016/j.ejpb.2007.01.020.
[35] P. Pathak, M. Nagarsenker, Formulation and Evaluation of Lidocaine Lipid Nanosystems for Dermal Delivery, AAPS PharmSciTech. 10 (2009) 985–992. doi:10.1208/s12249-009-9287-1.
[36] R.H. Müller, M. Radtke, S.A. Wissing, Solid lipid nanoparticles (SLN) and nanostructured lipid carriers (NLC) in cosmetic and dermatological preparations, in: Adv. Drug Deliv. Rev., 2002. doi:10.1016/S0169-409X(02)00118-7.
[37] S. Doktorovova, E.B. Souto, Nanostructured lipid carrier-based hydrogel formulations for drug delivery: a comprehensive review., Expert Opin. Drug Deliv. 6 (2009) 165–176. doi:10.1517/17425240802712590.
[38] C.H. Loo, M. Basri, R. Ismail, H.L.N. Lau, B.A. Tejo, M.S. Kanthimathi, H.A. Hassan, Y.M. Choo, Effect of compositions in nanostructured lipid carriers (NLC) on skin hydration and occlusion, Int. J. Nanomedicine. 8 (2013) 13–22. doi:10.2147/IJN.S35648.

[39] P. Desai, R.R. Patlolla, M. Singh, Interaction of nanoparticles and cell-penetrating peptides with skin for transdermal drug delivery, Mol. Membr. Biol. 27 (2010) 247–259. doi:10.3109/09687688.2010.522203.
[40] C. Guo, J. Wang, F. Cao, R.J. Lee, G. Zhai, Lyotropic liquid crystal systems in drug delivery, Drug Discov. Today. 15 (2010) 1032–1040. doi:10.1016/j.drudis.2010.09.006.
[41] M. Makai, E. Csányi, Z. Németh, J. Pálinkás, I. Eros, Structure and drug release of lamellar liquid crystals containing glycerol, in: Int. J. Pharm., 2003: pp. 95–107. doi:10.1016/S0378-5173(03)00066-8.
[42] V. Mathur, Y. Satrawala, M. Rajput, Physical and chemical penetration enhancers in transdermal drug delivery system, Asian J. Pharm. 4 (2010) 173. doi:10.4103/0973-8398.72115.
[43] A.R. Denet, R. Vanbever, V. Préat, Skin electroporation for transdermal and topical delivery, Adv. Drug Deliv. Rev. 56 (2004) 659–674. doi:10.1016/j.addr.2003.10.027.
[44] J.C. Weaver, Electroporation: A general phenomenon for manipulating cells and tissues, J. Cell. Biochem. 51 (1993) 426–435. doi:10.1002/jcb.2400510407.
[45] J. Gehl, Electroporation: Theory and methods, perspectives for drug delivery, gene therapy and research, Acta Physiol. Scand. 177 (2003) 437–447. doi:10.1046/j.1365-201X.2003.01093.x.
[46] B. Mali, T. Jarm, M. Snoj, G. Sersa, D. Miklavcic, Antitumor effectiveness of electrochemotherapy: A systematic review and meta-analysis, Eur. J. Surg. Oncol. 39 (2013) 4–16. doi:10.1016/j.ejso.2012.08.016.
[47] M. Belehradek, C. Domenge, B. Luboinski, S. Orlowski, J. Belehradek, L.M. Mir, Electrochemotherapy, a new antitumor treatment: First clinical Phase I-II trial, Cancer. 72 (1993) 3694–3700. doi:10.1002/1097-0142(19931215)72:12<3694::AID-CNCR2820721222>3.0.CO;2-2.
[48] L.F. Glass, M. Jaroszeski, R. Gilbert, D.S. Reintgen, R. Heller, Intralesional bleomycin-mediated electrochemotherapy in 20 patients with basal cell carcinoma, J. Am. Acad. Dermatol. 37 (1997) 596–599. doi:10.1016/S0190-9622(97)70178-6.
[49] R. Heller, M.J. Jaroszeski, D.S. Reintgen, C.A. Puleo, R.C. DeConti, R.A. Gilbert, L.F. Glass, Treatment of cutaneous and subcutaneous tumors with electrochemotherapy using intralesional bleomycin, Cancer. 83 (1998) 148–157. doi:10.1002/(SICI)1097-0142(19980701)83:1<148::AID-CNCR20>3.0.CO;2-W.
[50] J. Gehl, P.F. Geertsen, Efficient palliation of haemorrhaging malignant melanoma skin metastases by electrochemotherapy, Melanoma Res. 10 (2000) 585–589. doi:10.1097/00008390-200012000-00011.
[51] L.M. Mir, L.F. Glass, G. Sersa, J. Teissié, C. Domenge, D. Miklavcic, M.J. Jaroszeski, S. Orlowski, D.S. Reintgen, Z. Rudolf, M. Belehradek, R. Gilbert, M.P. Rols, J. Belehradek, J.M. Bachaud, R. DeConti, B. Stabuc, M. Cemazar, P. Coninx, R. Heller, Effective treatment of cutaneous and subcutaneous malignant tumours by electrochemotherapy., Br. J. Cancer. 77 (1998) 2336–42. doi:10.1038/bjc.1998.388.
[52] W.R. Panje, M.P. Hier, G.R. Garman, E. Harrell, A. Goldman, I. Bloch, Electroporation therapy of head and neck cancer, Ann Otol Rhinol Laryngol. 107 (1998) 779–85. doi:10.1177/000348949810700908.
[53] R. Heller, R. Gilbert, M.J. Jaroszeski, Clinical applications of electrochemotherapy, Adv. Drug Deliv. Rev. 35 (1999) 119–129. doi:10.1016/S0169-409X(98)00067-2.
[54] J.C. Visser, W.M.C. Dohmen, W.L.J. Hinrichs, J. Breitkreutz, H.W. Frijlink, H.J. Woerdenbag, Quality by design approach for optimizing the formulation and physical properties of extemporaneously prepared orodispersible films, Int. J. Pharm. 485 (2015) 70–76. doi:10.1016/j.ijpharm.2015.03.005.
[55] European Medicines Agency, ICH guideline Q8 (R2) on pharmaceutical development, EMA/CHMP/ICH/167068/2004. 8 (2015) 16706. doi:EMEA/CHMP/167068/2004 - ICH.
[56] R.-K. Chang, A. Raw, R. Lionberger, L. Yu, Generic Development of Topical Dermatologic Products, Part II: Quality by Design for Topical Semisolid Products, AAPS J. 15 (2013) 674–683. doi:10.1208/s12248-013-9472-8.
[57] E. Pallagi, R. Ambrus, P. Szabó-Révész, I. Csóka, Adaptation of the quality by design concept in early pharmaceutical development of an intranasal nanosized formulation, Int. J. Pharm. 491 (2015) 384–392. doi:10.1016/j.ijpharm.2015.06.018.

[58] A. Kovács, S. Berkó, E. Csányi, I. Csóka, Development of nanostructured lipid carriers containing salicyclic acid for dermal use based on the Quality by Design method, Eur. J. Pharm. Sci. 99 (2017) 246–257. doi:10.1016/j.ejps.2016.12.020.
[59] B. Shah, D. Khunt, H. Bhatt, M. Misra, H. Padh, Intranasal delivery of venlafaxine loaded nanostructured lipid carrier: Risk assessment and QbD based optimization, J. Drug Deliv. Sci. Technol. 33 (2016) 37–50. doi:10.1016/j.jddst.2016.03.008.
[60] U. S. Food and Drug Administration/Center for Biologics Evaluation and Research, Guidance for Industry. Q9 Quality Risk Management, Food Drug Adm. (2006) 1–72. https://www.fda.gov/downloads/Drugs/Guidances/ucm073511.pdf.
[61] N.A. Charoo, A.A.A. Shamsher, A.S. Zidan, Z. Rahman, Quality by design approach for formulation development: A case study of dispersible tablets, Int. J. Pharm. 423 (2012) 167–178. doi:10.1016/j.ijpharm.2011.12.024.
[62] U. S. Food and Drug Administration/Center for Biologics Evaluation and Research, Guidance for Industry. Q9 Quality Risk Management, Food Drug Adm. (2006) 1–72.
[63] G.E. Flaten, Z. Palac, A. Engesland, J. Filipović-Grčić, Ž. Vanić, N. Škalko-Basnet, In vitro skin models as a tool in optimization of drug formulation, Eur. J. Pharm. Sci. 75 (2015) 10–24. doi:10.1016/j.ejps.2015.02.018.
[64] G. Oliveira, A.E. Beezer, J. Hadgraft, M.E. Lane, Alcohol enhanced permeation in model membranes. Part I. Thermodynamic and kinetic analyses of membrane permeation, Int. J. Pharm. 393 (2010) 61–67. doi:10.1016/j.ijpharm.2010.03.062.
[65] D. Karadzovska, J.E. Riviere, Assessing vehicle effects on skin absorption using artificial membrane assays, Eur. J. Pharm. Sci. 50 (2013) 569–576. doi:10.1016/j.ejps.2013.02.020.
[66] B. Sinkó, J. Kökösi, A. Avdeef, K. Takács-Novák, A PAMPA study of the permeability-enhancing effect of new ceramide analogues, in: Chem. Biodivers., 2009: pp. 1867–1874. doi:10.1002/cbdv.200900149.
[67] A. Engesland, M. Skar, T. Hansen, N. Škalko-basnet, G.E. Flaten, New applications of phospholipid vesicle-based permeation assay: Permeation model mimicking skin barrier, J. Pharm. Sci. 102 (2013) 1588–1600. doi:10.1002/jps.23509.
[68] M. De Jager, W. Groenink, R. Bielsa I Guivernau, E. Andersson, N. Angelova, M. Ponec, J. Bouwstra, A novel in vitro percutaneous penetration model: Evaluation of barrier properties with P-aminobenzoic acid and two of its derivatives, Pharm. Res. 23 (2006) 951–960. doi:10.1007/s11095-006-9909-1.
[69] M. Van Gele, B. Geusens, L. Brochez, R. Speeckaert, J. Lambert, Three-dimensional skin models as tools for transdermal drug delivery: challenges and limitations, Expert Opin. Drug Deliv. 8 (2011) 705–720. doi:10.1517/17425247.2011.568937.
[70] A. de la Maza, A.M. Manich, L. Coderch, P. Bosch, J.L. Parra, The formation of liposomes in vitro by mixtures of lipids modeling the composition of the stratum corneum, Colloids Surfaces A Physicochem. Eng. Asp. 101 (1995) 9–19. doi:10.1016/0927-7757(95)03158-A.
[71] P.W. Wertz, W. Abraham, L. Landmann, D.T. Downing, Preparation of Liposomes from Stratum Corneum Lipids, J. Invest. Dermatol. 87 (1986) 582–584. doi:10.1111/1523-1747.ep12455832.
[72] C.M.S. Cereda, G.R. Tófoli, R.B. De Brito Junior, M.B. De Jesus, L.F. Fraceto, F.C. Groppo, D.R. De Araujo, E. De Paula, Stability and local toxicity evaluation of a liposomal prilocaine formulation, J. Liposome Res. 18 (2008) 329–339. doi:10.1080/08923970802500067.
[73] R.L. Biltonen, D. Lichtenberg, The use of differential scanning calorimetry as a tool to characterize liposome preparations, Chem. Phys. Lipids. 64 (1993) 129–142. doi:10.1016/0009-3084(93)90062-8.
[74] Y. Kaminoh, C. Tashiro, H. Kamaya, I. Ueda, Depression of phase-transition temperature by anesthetics: nonzero solid membrane binding, BBA - Biomembr. 946 (1988) 215–220. doi:10.1016/0005-2736(88)90395-1.
[75] H. Heerklotz, Interactions of surfactants with lipid membranes, Q. Rev. Biophys. 41 (2008) 205–264. doi:10.1017/S0033583508004721.

[76] N.L. Redman-Furey, M.J. Antinore, Determination of partition coefficients between dimyristoylphosphatidylcholine and water using differential scanning calorimetry, Anal. Chim. Acta. 251 (1991) 79–81. doi:10.1016/0003-2670(91)87118-Q.
[77] A.M. Kligman, E. Christophers, Preparation of Isolated Sheets of Human Stratum Corneum, Arch. Dermatol. 88 (1963) 702–705. doi:10.1001/archderm.1963.01590240026005.
[78] H. Patel, C. Tscheka, H. Heerklotz, Characterizing vesicle leakage by fluorescence lifetime measurements, Soft Matter. 5 (2009) 2849. doi:10.1039/b908524f.
[79] B. Godin, E. Touitou, Transdermal skin delivery: Predictions for humans from in vivo, ex vivo and animal models, Adv. Drug Deliv. Rev. 59 (2007) 1152–1161. doi:10.1016/j.addr.2007.07.004.
[80] E.C. Jung, H.I. Maibach, Animal models for percutaneous absorption, J. Appl. Toxicol. 35 (2015) 1–10. doi:10.1002/jat.3004.
[81] D. Marsh, Handbook of lipid bilayers, 2013. doi:10.1201/b11712.
[82] A.M. Panico, A. Santagati, V. Cardile, D. Urso, B. Gentile, G. Ronsisvalle, Calorimetric study on the interaction of thienopyrimidine derivatives with phosphatidylcholine membranes, Colloids Surfaces B Biointerfaces. 28 (2003) 77–81. doi:10.1016/S0927-7765(02)00118-2.
[83] B. Tenchov, On the reversibility of the phase transitions in lipid-water systems, Chem. Phys. Lipids. 57 (1991) 165–177. doi:10.1016/0009-3084(91)90074-L.
[84] T.B. Pedersen, S. Frokjaer, O.G. Mouritsen, K. Jørgensen, A calorimetric study of phosphocholine membranes mixed with desmopressin and its diacylated prodrug derivative (DPP), Int. J. Pharm. 233 (2002) 199–206. doi:10.1016/S0378-5173(01)00946-2.
[85] P. yuan Wang, J. wen Chen, F. Hwang, Anisodamine causes acyl chain interdigitation in phosphatidylglycerol, FEBS Lett. 332 (1993) 193–196. doi:10.1016/0014-5793(93)80511-R.
[86] I. Dierking, Textures of liquid crystals, Wiley-VCH, Weinheim, 2003.
[87] L. Voelker-Pop, Optical methods in rheology: Polarized light imaging, Chem. List. 108 (2014) 707–710.
[88] J. Zhang, Y. Fan, E. Smith, Experimental design for the optimization of lipid nanoparticles, J Pharm Sci. 98 (2009) 1813–1819. doi:10.1002/jps.21549.
[89] N. Anton, J.P. Benoit, P. Saulnier, Design and production of nanoparticles formulated from nano-emulsion templates-a review, J Control Release. 128 (2008) 185–199. doi:10.1016/j.jconrel.2008.02.007.
[90] H.M. Badawi, W. Forner, S.A. Ali, The conformational stability, solvation and the assignments of the experimental infrared, Raman, (1)H and (13)C NMR spectra of the local anesthetic drug lidocaine, Spectrochim Acta A Mol Biomol Spectrosc. 142 (2015) 382–391. doi:10.1016/j.saa.2015.02.005.
[91] C. Puglia, M.G. Sarpietro, F. Bonina, F. Castelli, M. Zammataro, S. Chiechio, Development, Characterization, and In Vitro and In Vivo Evaluation of Benzocaine- and Lidocaine-Loaded Nanostructrured Lipid Carriers, J. Pharm. Sci. 100 (2011) 1892–1899. doi:10.1002/jps.22416.
[92] L.B. Jensen, K. Petersson, H.M. Nielsen, In vitro penetration properties of solid lipid nanoparticles in intact and barrier-impaired skin, Eur J Pharm Biopharm. 79 (2011) 68–75. doi:10.1016/j.ejpb.2011.05.012.
[93] P. You, R. Yuan, C. Chen, Design and evaluation of lidocaine- and prilocaine-coloaded nanoparticulate drug delivery systems for topical anesthetic analgesic therapy: A comparison between solid lipid nanoparticles and nanostructured lipid carriers, Drug Des. Devel. Ther. 11 (2017) 2743–2752. doi:10.2147/DDDT.S141031.
[94] P. Pathak, M. Nagarsenker, Formulation and evaluation of lidocaine lipid nanosystems for dermal delivery, AAPS PharmSciTech. 10 (2009) 985–992. doi:10.1208/s12249-009-9287-1.
[95] M. Franz-Montan, D. Baroni, G. Brunetto, V.R.V. Sobral, C.M.G. da Silva, P. Venâncio, P.W. Zago, C.M.S. Cereda, M.C. Volpato, D.R. de Araújo, E. de Paula, F.C. Groppo, Liposomal lidocaine gel for topical use at the oral mucosa: characterization, in vitro assays and in vivo anesthetic efficacy in humans., J. Liposome Res. 25 (2014) 11–19. doi:10.3109/08982104.2014.911315.

[96] S. Babaei, S. Ghanbarzadeh, Z.M. Adib, M. Kouhsoltani, S. Davaran, H. Hamishehkar, Enhanced skin penetration of lidocaine through encapsulation into nanoethosomes and nanostructured lipid carriers: A comparative study, Pharmazie. 71 (2016) 247–251. doi:10.1691/ph.2016.5158.
[97] L. H., Oleogels – what non-aqueous products canaccomplish, Kosmet. Prax. 4 (2004).
[98] S. Wissing, A. Lippacher, R. Muller, Investigations on the occlusive properties of solid lipid nanoparticles (SLN), J Cosmet Sci. 52 (2001) 313–324. http://www.ncbi.nlm.nih.gov/pubmed/11567210.
[99] M. Foldvari, Non-invasive administration of drugs through the skin: challenges in delivery system design, Pharm Sci Technolo Today. 3 (2000) 417–425. http://www.ncbi.nlm.nih.gov/pubmed/11116201.
[100] H. Iwai, J. Fukasawa, T. Suzuki, A liquid crystal application in skin care cosmetics, Int J Cosmet Sci. 20 (1998) 87–102. doi:10.1046/j.1467-2494.1998.171741.x.
[101] O. Akkus, Evaluation of Skin and Subcutaneous Adipose Tissue Thickness for Optimal Insulin Injection, J. Diabetes Metab. 3 (2012). doi:10.4172/2155-6156.1000216.
[102] K. Robertson, J.L. Rees, Variation in epidermal morphology in human skin at different body sites as measured by reflectance confocal microscopy, Acta Derm. Venereol. 90 (2010) 368–373. doi:10.2340/00015555-0875.
[103] Y. Niu, X. Cao, F. Song, T. Xie, X. Ji, M. Miao, J. Dong, M. Tian, Y. Lin, S. Lu, Reduced Dermis Thickness and AGE Accumulation in Diabetic Abdominal Skin, Int. J. Low. Extrem. Wounds. 11 (2012) 224–230. doi:10.1177/1534734612457570.
[104] A. Synytsya, P. Alexa, J. Besserer, J. De Boer, S. Froschauer, R. Gerlach, M. Loewe, M. Moosburger, I. Obstova, P. Quicken, B. Sosna, K. Volka, M. Würkner, Raman spectroscopy of tissue samples irradiated by protons, Int. J. Radiat. Biol. 80 (2004) 581–591. doi:10.1080/09553000412331283515.
[105] M.A. Sallam, A.M. Motawaa, S.M. Mortada, An insight on human skin penetration of diflunisal: lipogel versus hydrogel microemulsion, Drug Dev. Ind. Pharm. 41 (2015) 141–147. doi:10.3109/03639045.2013.850711.
[106] R. Rajabalaya, M.N. Musa, N. Kifli, S.R. David, Oral and transdermal drug delivery systems: Role of lipid-based lyotropic liquid crystals, Drug Des. Devel. Ther. 11 (2017) 393–406. doi:10.2147/DDDT.S103505.
[107] S. Nie, W.W. Hsiao, W. Pan, Z. Yang, Thermoreversible pluronic F127-based hydrogel containing liposomes for the controlled delivery of paclitaxel: In vitro drug release, cell cytotoxicity, and uptake studies, Int. J. Nanomedicine. 6 (2011) 151–166. doi:10.2147/IJN.S15057.
[108] I.B. Pathan, C. Mallikarjuna Setty, Enhancement of transdermal delivery of tamoxifen citrate using nanoemulsion vehicle, Int. J. PharmTech Res. 3 (2011) 287–297.
[109] Z. Ujhelyi, F. Fenyvesi, J. Váradi, P. Fehér, T. Kiss, S. Veszelka, M. Deli, M. Vecsernyés, I. Bácskay, Evaluation of cytotoxicity of surfactants used in self-micro emulsifying drug delivery systems and their effects on paracellular transport in Caco-2 cell monolayer, Eur. J. Pharm. Sci. 47 (2012) 564–573. doi:10.1016/j.ejps.2012.07.005.
[110] L. Kiss, F.R. Walter, A. Bocsik, S. Veszelka, B. Ózsvári, L.G. Puskás, P. Szabó-révész, M.A. Deli, Kinetic analysis of the toxicity of pharmaceutical excipients cremophor EL and RH40 on endothelial and epithelial cells, J. Pharm. Sci. 102 (2013) 1173–1181. doi:10.1002/jps.23458.
[111] Y. Li, C. Dong, D. Cun, J. Liu, R. Xiang, L. Fang, Lamellar Liquid Crystal Improves the Skin Retention of 3-O-Ethyl-Ascorbic Acid and Potassium 4-Methoxysalicylate In Vitro and In Vivo for Topical Preparation., AAPS PharmSciTech. 17 (2016) 767–77. doi:10.1208/s12249-015-0353-6.
[112] D.G. Lim, W.W. Jeong, N.A. Kim, J.Y. Lim, S.H. Lee, W.S. Shim, N.G. Kang, S.H. Jeong, Effect of the glyceryl monooleate-based lyotropic phases on skin permeation using invitro diffusion and skin imaging, Asian J. Pharm. Sci. 9 (2014) 324–329. doi:10.1016/j.ajps.2014.06.008.
[113] B. Li, Z.-Q. Ge, Nanostructured Lipid Carriers Improve Skin Permeation and Chemical Stability of Idebenone, AAPS PharmSciTech. 13 (2012) 276–283. doi:10.1208/s12249-011-9746-3.

ACKNOWLEDGMENTS

Firstly, I would like to express my sincere gratitude to the Head of the Institute of Pharmaceutical Technology and Regulatory Affairs, **Dr. habil. Ildikó Csóka Ph.D.** and the Head of the Pharmaceutical Technology Ph.D. Program, **Professor Piroska Szabó-Révész** for providing me the opportunity to work in this department and to complete my work under their expert guidance.

I am also enormously grateful to my supervisors **Dr. habil. Erzsébet Csányi Ph.D.**, Associate Professor, and **Dr. Szilvia Berkó Ph.D.**, Senior Lecturer, for the continuous support of my Ph.D study and related research, for their patience, motivation, and immense knowledge

I would like to express my kindest thanks to my **co-authors** for their kind collaboration, especially my colleagues at the Institute of Pharmaceutical Technology and Regulatory Affairs, **Attila Gácsi** and **Anita Kovács** for their co-operation and help.

My sincere thanks also go to **Professor Heiko Heerklotz**, Department of Pharmaceutical Technology and Biopharmacy, University of Freiburg, who provided me with the opportunity to join their team as an intern, and who gave access to the laboratory and research facilities and helped me with his valuable advice.

I would also like to thank **all members of the Institute of Pharmaceutical Technology and Regulatory Affairs** for their help and friendship.

Finally, I would like to thank **my family and friends** for providing me with unfailing support and continuous encouragement throughout my years of study and through the process of researching and writing this thesis. This accomplishment would not have been possible without them. Thank you.